On the Design of Single Electron Transistors for the Measurement of Spins in Phosphorus Doped Silicon

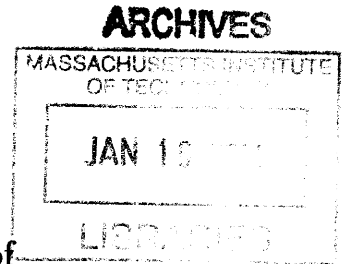

by

Mallika Randeria

Submitted to the Department of Physics

in partial fulfillment of the requirements for the degree of

Bachelor of Science in Physics

at the

MASSACHUSETTS INSTITUTE OF TECHNOLOGY

June 2012

© Mallika Randeria, MMXII. All rights reserved.

The author hereby grants to MIT permission to reproduce and to distribute publicly paper and electronic copies of this thesis document in whole or in part in any medium now known or hereafter created.

Author ....

Department of Physics
May 11, 2012

Certified by ....

Amir Yacoby
Professor of Physics, Harvard University
Thesis Supervisor

Certified by ....

Pablo Jarillo-Herrero
Assistant Professor of Physics, MIT
Thesis Supervisor

Accepted by ....

Nergis Mavalvala
Senior Thesis Coordinator, Department of Physics

On the Design of Single Electron Transistors for the Measurement of Spins in Phosphorus Doped Silicon

by

Mallika Randeria

Submitted to the Department of Physics
on May 11, 2012, in partial fulfillment of the
requirements for the degree of
Bachelor of Science in Physics

Abstract

Phosphorus doped silicon is a prime candidate for spin based qubits. We plan to investigate a novel hybrid technique that combines the advantages of spin selective optical excitations with that of electrical readout measurements to detect spin defects in semiconductors. In this thesis, I present my work on the design and fabrication of single electron transistors (SETs) for the electrical readout of the spin state of phosphorus doped silicon. For such highly sensitive measurements, it is necessary for the characteristic energy of the SET to be larger than thermal fluctuations. My goal was to design and fabricate SETs on P doped Si that function at temperatures of about 2K. This necessitated minimizing the tunnel junction area through optimized lithography and evaporation procedures. I have produced SETs with charging energies of $\sim$ 0.85 meV corresponding to a temperature of $\sim$ 10 K. These SETs have a charge sensitivity of $\sim 2 \times 10^{-4}\ e/\sqrt{\text{Hz}}$ at 10 mK but have yet to be tested at temperatures of 2K. The mechanism of detection involves exciting the P donor to a P^+ ion that then shifts the electrochemical potential near the SET, creating a sharp peak in the current through the SET. This can ultimately be used for single shot readout and thus for a measurement of the spin state of the electron - a promising system for quantum computation, magnetometry and spintronics.

Thesis Supervisor: Amir Yacoby
Title: Professor of Physics, Harvard University

Thesis Supervisor: Pablo Jarillo-Herrero
Title: Assistant Professor of Physics, MIT

Acknowledgments

The vibrant atmosphere in Cambridge, with no dearth of intellectual opportunities, gave me the chance to be a part of not one but two great institutions during my time here in Boston.

Working at Harvard with Amir's group has been one of my most fulfilling research experiences. I have learned so much from working in the Yacoby group, especially through my interactions with all the wonderful group members. I will cherish my memories of the Yacoby group and the sense of camaraderie that brings the lab together. I would not be doing condensed matter if it werent for my time spent working in the Yacoby group.

Special thanks to Amir for giving me the opportunity to work in his group and the chance to work on an independent project of my own. Through conversations with Amir, I have learned a lot about physics as well as how to move my research forward. Additionally, I have greatly benefited from Amir's advice about grad schools.

I would like to thank Vivek for training me during my early days in the lab. His knowledge of just about everything made him a great resource. Under his guidance, I learned how to approach problem solving in the lab. He was ever-ready to take the time to discuss physics with me, and I have really grown as a scientist through our interactions.

It has been a great pleasure to work closely with Lan on this experiment. Being new to the lab, I have been able to accomplish much more working with Lan, than I would have on my own. She has been extremely helpful in pushing the fabrication process along, and has always been available to answer questions about the experimental setup. More recently, it has been great to have Susanne join our team, giving us one more person to bounce ideas off of. I also really appreciate the discussions I had with Vivek, Oliver, Susanne and Lan with regard to this thesis project.

It wasnt long after my arrival at MIT that I was drawn to the MIT physics community. Here I have learned and enjoyed physics, stretched myself and grown tremendously as a scientist and as a person. I would like to thank my many mentors

who helped me explore and discover the mysteries of physics: Vladan, for training me as a UROP student for the year prior to joining Amirs group; Nergis and Sean for their tireless efforts in J-lab which helped me discover my passion for table-top experimental physics. In addition, I would like to thank Tali for being a resourceful and insightful academic advisor.

I would like to thank all my friends, for providing a sense of balance in my life outside of physics. Their support and kindness have allowed me to flourish at MIT-making my short four years unforgettable.

Last but not least, I would like to thank my parentsthe pillars in my life. Their unconditional love and support has sustained me through MIT and instilled in me a sense of confidence to tackle bigger problems in the future.

I dedicate this thesis to my sister as she begins her undergraduate career. May she find the same passion for physics that I discovered.

Contents

1 Introduction **9**

1.1 Motivation for the Experiment 9

1.2 Main Results 11

1.3 Thesis Overview 13

2 Background for Experiment and Measurement Scheme **14**

2.1 Silicon 14

2.2 Phosphorus doped Silicon 15

2.3 P doped Si Sample 19

2.4 Experiment Setup 19

3 Single Electron Transistor Theory **22**

3.1 The Push Towards Single Electron Devices 22

3.2 The Quantum Dot 24

3.3 Charge Quantization for a Tunnel Junction 27

3.4 Electron Transport Through an SET 28

3.5 Role of SETs in P doped Si experiment 35

4 SET Fabrication **37**

4.1 Ohmic Contacts 39

4.2 Electron Beam Lithography 41

4.3 Shadow Evaporation 43

4.4 Dose Test 45

4.5 Resist Thickness and Angle Determination 46
4.6 Focus and Alignment Problems 49
4.7 Successful SETs 50

5 SET Characterization 53
5.1 Preliminary Measurements 53
5.2 Measurement of Coulomb Blockade in SETs 54
5.3 Charge Sensitivity of SETs 57
5.4 Future Testing 61

6 Conclusion 62

A SET Fabrication Recipes 64
A.1 Photolithography of Optical Gates 64
A.2 Ebeam Lithography 65

List of Figures

1-1 Main Result: Coulomb Diamond Data for SETs 12

2-1 Cubic Structure of Silicon 15

2-2 Band Structure of Silicon 16

2-3 Transition between donor and donor-bound exciton states 18

2-4 Spectrum of phosphorus-bound-exciton transitions 19

2-5 Experiment Setup 21

3-1 Circuit diagram of a single electron transistor 23

3-2 Schematic of tunneling of an electron through an SET 29

3-3 Energy parabolas for an SET 30

3-4 Schematic illustrating Coulomb blockade 31

3-5 Schematic representation of conductance through a quantum dot . . . 33

3-6 Schematic representation of current flow through an SET 35

3-7 Schematic of Coulomb blockade diamonds 36

4-1 Schematic of an SET 38

4-2 Image of file used in SET fabrication 38

4-3 Schematic of photolithography procedure 40

4-4 Image of file used to specify SET features 42

4-5 Schematic of SET angle evaporation 44

4-6 Determination of critical evaporation angle 45

4-7 SEM image of dose test pattern 46

4-8 SEM image of dose test results 47

4-9 SET evaporation at less than critical angle 48
4-10 SEM image of mesa with unsuccessful liftoff 49
4-11 SEM image of a broken SET island 49
4-12 SEM image of SET alignment to ohmic contacts 50
4-13 SEM image of successful SETs with narrow features 51
4-14 SEM image of successful SETs but with bad ohmic contacts 51
4-15 SEM image of successful sample tested in dilution refrigerator 52

5-1 Measurement of Coulomb blockade diamonds 56
5-2 Measurement 1 for charge sensitivity determination 58
5-3 Measurement 2 for charge sensitivity determination 60

Chapter 1

Introduction

1.1 Motivation for the Experiment

Quantum information offers new paradigms with the promise to revolutionize computing and cryptography. This vision can only be realized with the ability to coherently control and manipulate quantum systems. While a classical bit can be either 0 or 1, quantum bits (qubits) can exist in a superposition of these classical states simultaneously. The potential for feasible qubits was first seen in atomic physics, where the internal levels of atoms and ions present a natural set of quantum states. These states are isolated using laser cooling and cavity modes and manipulated using optical transitions. Solid-state systems are now emerging as promising candidates for electron and nuclear spin-based qubits. The ideas developed in the context of atomic systems can be readily applied in the solid state, which offer additional advantages in terms of modern fabrication techniques, scalability, tunability and integration with existing technology.

The primary challenge of using spins as qubits lies in the detection of a single spin. Most single qubit measurement schemes use either optical or electrical methods for both initialization and readout. However, due to low detection efficiencies and noisy backgrounds, these methods have severe bottlenecks. We plan to investigate a novel hybrid technique that combines the advantages of spin selective optical excitations with that of electrical readout measurements to detect spin defects in solid state sys-

tems. We focus on the measurement of individual electron spins of phosphorus-doped silicon and ultimately hope to achieve single shot readout of the electron spin state which means that once the spin is initialized, its readout occurs within a coherence time.

Phosphorus-doped silicon is a prime candidate for spin based qubits for a variety of reasons. Given its ubiquity in the semiconductor industry, Si samples are readily available and fabrication techniques are well established. The weak spin orbit coupling in silicon gives rise to long coherence times, an essential feature for information storage in a qubit [22]. Additionally, P doped Si is an example of a solid state system with a spin selective optical transition that can be exploited for initialization of the qubit. A narrow linewidth laser is used to optically excite the P donor from the neutral state to the excited donor-bound exciton state [4]. A specific spin state of the donor can be isolated by using a small 1-2 Tesla magnetic field to Zeeman split the spin degeneracy of the electrons. This gives us the ability to address a P valence electron in a particular spin state by tuning the laser frequency appropriately.

The excited donor-bound-exciton state decays most often via the Auger process, ionizing the donor, ejecting an electron and leaving behind a P^+ ion [19]. One could choose to optically readout the ejected electron. However, this would result in a rather weak emission signal from a single donor over a broad frequency range, making single shot readout impractical. We therefore turn to using electrical detection methods to see whether the P atom was ionized or not. We do so using single electron transistors (SETs).

An SET is a nonlinear, nano-electronic device consisting of two tunnel junctions, a source and a drain, capacitively coupled to a small island of electrons [12]. This device is capable of highly sensitive measurements of the local charge. In the regime where the energy levels of the source and the drain are below the potential of the island, electron tunneling from source to drain is forbidden. However, the presence of the P^+ ion shifts the potential of the island [19]. This results in a sharp peak in the current through the SET that can be used for single shot readout and thus for a measurement of the spin state of the electron [5].

The presence of a nuclear spin of the P atom, in addition to the spin of the electron, gives rise to the possibility of exploiting the hyperfine splitting for information storage. The considerably longer coherence times of the P nucleus opens the door for exploring entanglement of multiple qubits, essential for harnessing the power of quantum information processing, and the possibility of scalable quantum computers [11]. Another novel application of this system is in the realm of high precision magnetometry to measure very small magnetic fields measured through modulations of local Zeeman shifts [19]. Additionally, this hybrid technique of optical initialization and electrical readout is very versatile and can be extended to other solid state systems such as nitrogen vacancy centers in diamond.

1.2 Main Results

My senior thesis project involved designing and fabricating singe electron transistors (SETs) for electrical readout of the spin state of the P donor in Si. The ability to use an SET for a highly sensitive measurement requires the characteristic charging energy, E_C, of the SETs to be much larger than the thermal energy of the charge carriers. Therefore the experiment will be conducted in a cryostat which is capable of consistently reaching a stable temperature of $\sim$ 1.5K. Thus my ultimate goal was to fabricate SETs on P doped Si samples that function at temperatures of about 2K. This necessitated minimizing the tunnel junction area through optimized lithography and evaporation procedures in order to decrease the capacitance and therefore increase the charging energy. These SETs were tested in a dilution refrigerator at a temperature of 10mK. We see very nice Coulomb oscillations and Coulomb blockade diamonds as we sweep the bias and gate voltages as shown in Fig. 1-1. Each oscillation is indicative of a single electron tunneling onto the island. I have successfully produced SETs with charging energies of $\sim$ 0.85 meV corresponding to a temperature of $\sim$ 10 K. These SETs have a charge sensitivity of 2×10^{-4} $e/\sqrt{\text{Hz}}$ at 10 mK. They will be tested at temperatures of 2K once our cryostat arrives.

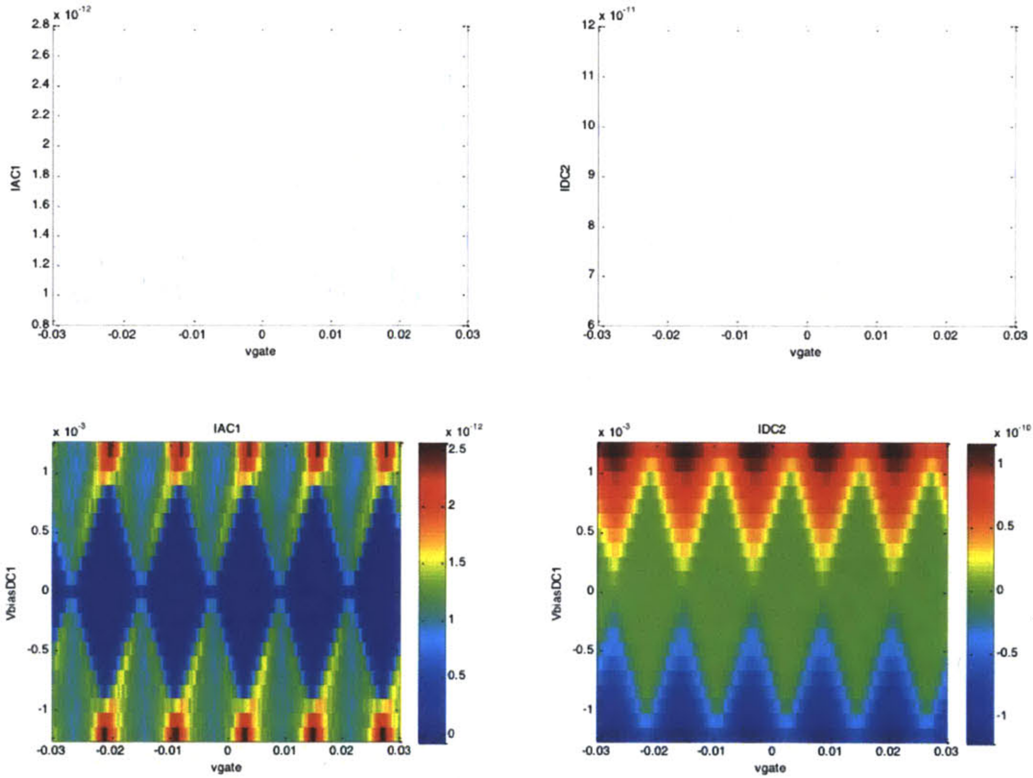

Figure 1-1: SET characterization measurement showing Coulomb oscillations (a), (c) and Coulomb blockade diamonds (b), (d) at a temperature of 10mK. The data shows the differential conductance (left) and DC conductance (right) as we sweep the gate voltage shown on the x-axis) and bias voltage (y-axis). The blockade region is the region in the diamonds where there is zero conductance.
Panels bd is the map of conductane as

1.3 Thesis Overview

This thesis is organized as follows. Chapter 2 contains some of the theory behind the experiment, background information on the experimental setup as well as the expected measurement scheme. In Chapter 3 of this thesis, I present the theory of electron transport through a single electron transistor and discuss how it can be used for very sensitive charge detection. In Chapter 4, I describe the fabrication procedures that I developed for producing SETs. Chapter 5 shows measurements made to characterize the operating temperature and sensitivity of these SETs. Finally, in Chapter 6, I summarize the results of my experiment and discuss the future directions of the experiment.

Chapter 2

Background for Experiment and Measurement Scheme

In our experiment, we plan to investigate a novel hybrid technique that combines the advantages of spin selective optical excitations with that of electrical readout measurements to detect spin defects in solid state systems. The measurements focus on individual electron spins of phosphorus-doped silicon and ultimately hope to achieve single shot readout of the electron spin state which means that once the spin is initialized, its readout occurs within a coherence time. In this chapter, I discuss the theory needed to understand the general setup of our experiment and then move on to describing the proposed experimental setup. I start with a little bit of background on silicon. I then describe phosphorus doped silicon, and its spin selective optical transition. Next I briefly discuss the P doped Si samples used in the experiment. Finally, I sketch the setup used to measure the spin state of the electron and briefly talk about the measurement scheme.

2.1 Silicon

Silicon (Si) has a diamond crystal structure which can be described by a face-centered cubic lattice with two atoms per unit cell. The basis consists of two atoms located at $(0,0,0)$ and $(\frac{a}{4}, \frac{a}{4}, \frac{a}{4})$, with the lattice constant for silicon, a being 5.43 Å. The

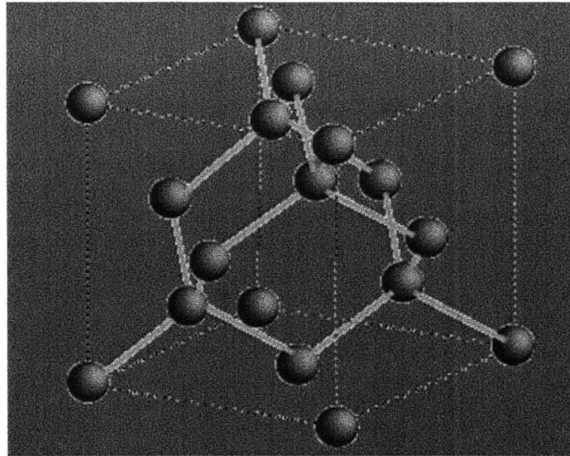

Figure 2-1: A unit cell of the face-centered cubic lattice for silicon. Taken from [21].

structure is shown in Fig. 2-1 where each atom sits at the center of a tetrahedron built from its four nearest neighbors.

The band structure of silicon is shown in Fig. 2-2 (a). Silicon has an indirect band gap, where the minimum of the conduction band occurs at $\mathbf{k} = 0.85(2\pi/a)(1,0,0)$ [8]. Thus there are six symmetry-related equivalent minima in the Brillouin zone. These constant-energy surfaces near the conduction band minima are ellipsoidal pockets with the long axes directed along the $\langle 100 \rangle$ directions shown in Fig. 2-2 (b) [1]. The valence band minimum occurs at $\mathbf{k} = 0$ where the degenerate "light hole" and "heavy hole" bands with different effective masses meet.

2.2 Phosphorus doped Silicon

The phosphorus (P) substitutional dopant in Si supplies additional electrons to the conduction band, which act as donors. When a P atom with electronic configuration ($3s^2$ $3p^3$) substitutes for Si atom ($3s^2$ p^2) it acts as an additional positive charge with an extra electron bound to it and can effectively be modeled as a hydrogen-like atom embedded in the Si lattice. To first approximation, if we ignore the difference in structure between the phosphorus and silicon ion cores, the phosphorus can be considered as an additional positive charge placed on a Si site, along with an additional

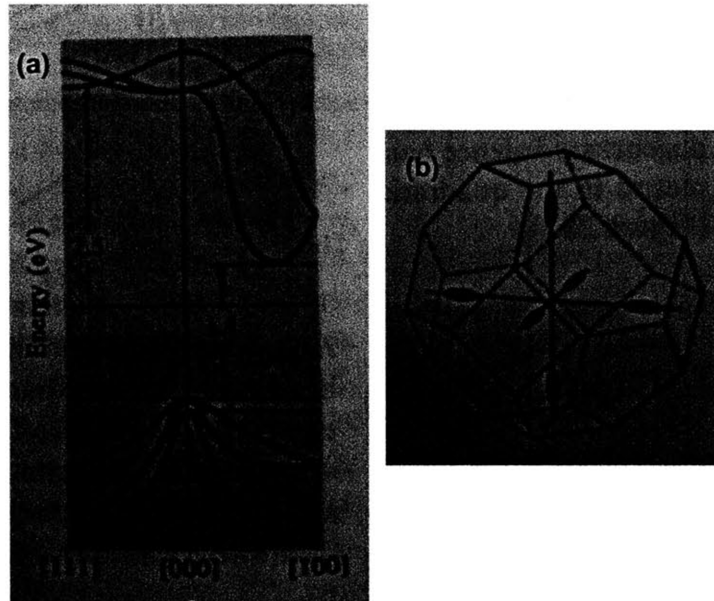

Figure 2-2: (a) Illustration of the band structure of silicon in reciprocal space. Note the indirect band gap of 1.1 eV between the conduction band minimum along [100] and the valence band maximum at [000]. In the valence band, the heavy hole and light hole bands with different effective masses as well as a third band that is split off due to spin-orbit coupling are shown.(b) Six-symmetry related instant energy ellipsoidal pockets in the conduction band. Taken from [1].

electron. This gives rise to a screened Coulomb potential between the the extra donor electron and the P nucleus.

We estimate the binding energy of the donor electron around the P+ ion to be

$$E_b = \frac{m^*}{m_e}\frac{1}{(\epsilon/\epsilon_0)^2} \times 13.6\ eV, \tag{2.1}$$

where m_e is the mass of the electron, m^* is the effective mass, ϵ_0 is the permittivity of free space and ϵ is the dielectric constant. The radius of the bound state is $r_0 = (m/m^*)(\ \epsilon/\epsilon_0)\ a_0$, where $a_0 = 0.53\ \mathring{A}$ is the Bohr radius of the Hydrogen atom. Using $m^* = 0.3m$ and $\epsilon = 12\epsilon_0$ for Si gives a binding energy $E_b = 45meV \approx 52K$ [1]. These corrections lead to a binding energy of the donor electron that is greatly reduced compared to that of a hydrogen atom. Thus the electron donor is loosely bound to the P atom can be ionized into the conduction band depending on the temperature [1].

Typically, in semiconductors, a photon with energy above the band gap excites an electron from the valence band to the conduction band, leaving behind a hole in the valence band. An exciton is a negatively charged electron bound by the Coulomb interaction to a positively charged hole. The lifetime of an exciton ranges from nanoseconds to milliseconds after which the electron and hole recombine to emit a photon of characteristic energy. In indirect band gap semiconductors such as silicon, this process is assisted by a wave vector conserving phonon [1].

Phosphorus doped Silicon is an example of a solid state systems with a spin selective optical transition between the neutral P donor state to the donor-bound-exciton state. The ground state of the P neutral donor state, D^0, consists of the positive P donor ion bound to the donor electron. The donor-bound-exciton D^0X consists of two interacting electrons and one hole, as well as the fixed positive donor ion. It is energetically favorable for these two electrons to form a spin-singlet. Since the absorption of a photon gives rise to the donor-bound-exciton state, in order to conserve momentum, the hole has $J_h = 3/2$ making its wave function four fold degenerate. A schematic is shown in Fig. 2-3.

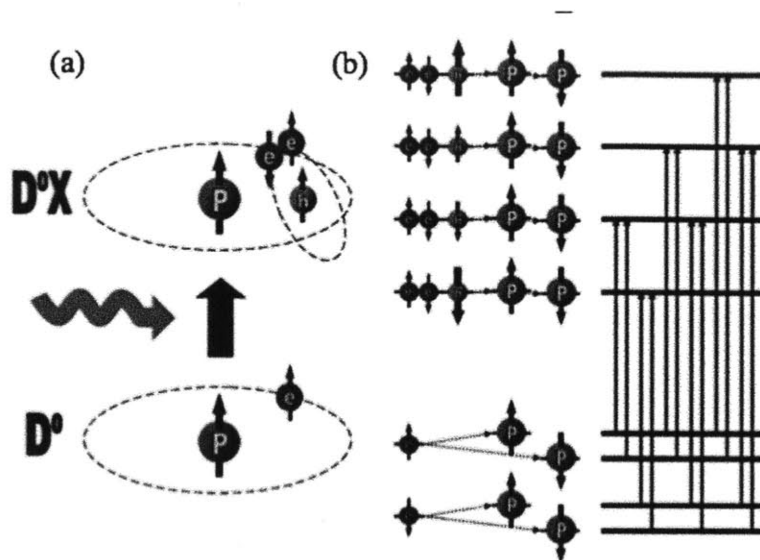

Figure 2-3: (a) Optical transition between the donor (D^0) and the donor-bound-exciton (D^0X) states. The electrons form a singlet. (b) The Zeeman splitting of the states in the presence of a magnetic field. Taken from [19].

In this system, the Auger process dominates the relaxation, where energy resulting from the recombination of the electron hole pair is used to ionize the donor, leaving behind an ionized P^+ and an energetic free electron [19].

A weak magnetic field of 1-2 Tesla is applied to the sample in order to Zeeman split both the ground and excited states. The applied field lifts the donor electron spin degeneracy of the D^0 ground state, splitting it into two levels determined by the projection of the electron spin. Technically, the hyperfine interaction between the electron and nuclear spins can also be resolved. The current experiment is focused on the spin of the electron but can be extended in the future to take the hyperfine interaction into account. The D^0X state has two electrons in a spin singlet state. Thus, in the presence of a magnetic field, the $J_h = 3/2$ spin of the hole determines the level splitting, splitting into four Zeeman levels [4]. The Zeeman spectrum of the phosphorus bound exciton transitions is shown in Fig. 2-4.

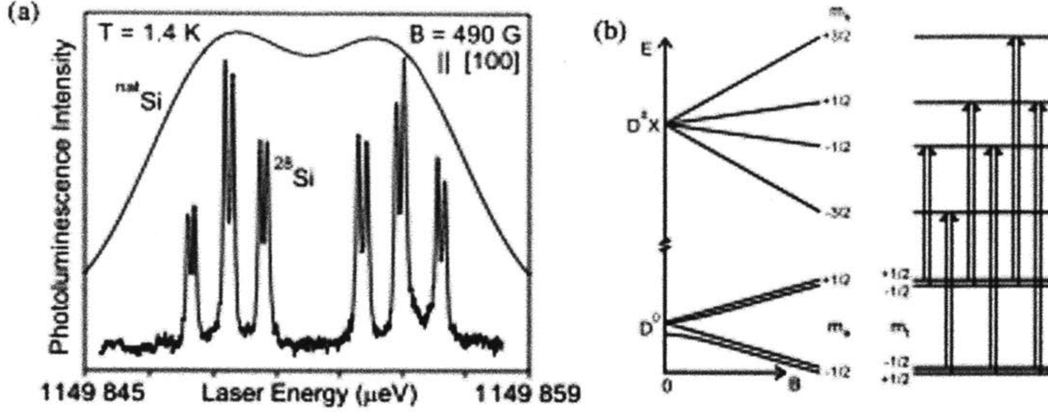

Figure 2-4: (a) Spectrum of phosphorus-bound-exciton transitions in isotopically purified Silicon. The six doublet transitions allowed by selection rules are shown in (b). They are ordered in increasing energy from left to right in correspondence with the ones shown in (a). Taken from [4].

2.3 P doped Si Sample

We use single electron transistors (SETs) to detect whether a P atom was ionized via the Auger process. We pattern these SETs directly onto the P doped Si sample. Ideally we would like to have the SETs as close to the P dopants as possible. We ordered neutron transmutation doped (NTD) Si wafers from Silicon Quest International. These wafers offer an advantage in terms of better spatial distribution of the dopants. The NTD process involves irradiating neutrons into an undoped, highly purified silicon sample. Through radioactive decay a Si atom transmutes into a ^{31}P atom. The sample has a 500 Ohm-cm resistivity with 8×10^{12} P atoms / cm^3 Si with a spacing of 500 nm/P atom. The 4 inch wafer is 375 μm thick with a single side polished. Preliminary testing of SETs was done on ordinary P doped Si samples with resistivities of 1-10 Ohm-cm.

2.4 Experiment Setup

As discussed in the introduction, the ultimate goal of this experiment is to implement a hybrid optical initialization with electrical readout scheme. The plan for the setup

of our experiment looks something like Fig. 2-5. The experiment is in the early stages of being set up. The first step involves fabricating SETs on the P doped Si sample. After fabrication, the sample will be placed in a cryostat in order to cool the sample and achieve temperatures below the charging energy of the SET. The cryostat is a pumped helium (4K) system with a 2T magnet. In the dynamic flow regime, the temperature can consistently remain stable at $\sim$ 1.5K. This temperature is the limiting factor for our SET charging energy. The cryostat has been ordered and is to arrive soon (by the end of May 2012).

The sample is then optically excited using a near infrared 1078nm Yb-doped Fiber laser. We thermo-piezo-electrically tune the laser to one of the specific transition shown in Fig. 2-4. A wave meter is used to precisely monitor the frequency of the laser. The laser is mechanically chopped in order to allow for the elimination of noise from all sources except the donor-bound-exciton decay. This blocking and unblocking of the laser gives us the ability to perform an AC measurement of the effects of the excitation laser on the P donors of the sample. The electron only gets excited if it is in the spin state with the same frequency as the laser frequency to which we have tuned. If the two frequencies are the same, the donor ($P^+ + e^-$) will be excited, form a donor-bound-exciton ($P^+ + e^- + e^- + h^+$), and then decay via the Auger process. We ultimately wish to detect the spin state of the electron, i.e. whether the laser frequency was able to excite the donor. This is done by using the SET to electrically detect the charge of the the P, i.e. whether the P donor was ionized via the Auger process or not.

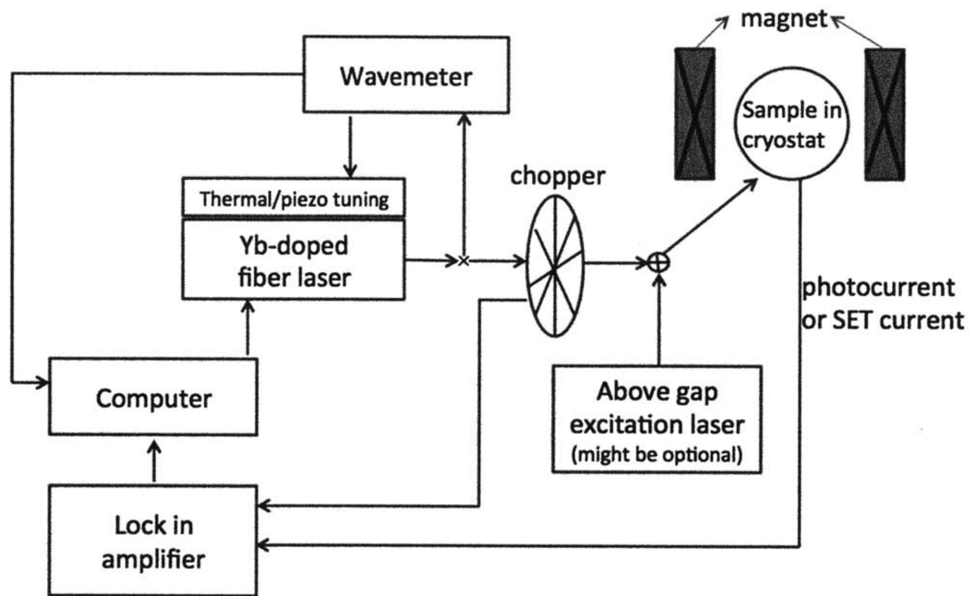

Figure 2-5: Schematic diagram showing the setup of the experiment. The P doped Si sample with fabricated SETs is placed in a helium cryostat. The donors are optically excited using a narrow linewidth laser which can be tuned to a desired frequency. The SETs are then used to detect whether the donor was ionized.

Chapter 3

Single Electron Transistor Theory

This chapter presents the details of electron transport through a single electron transistor (SET) by examining the roles played by each of the different components of an SET. I start with the motivation for the push towards exploiting quantum mechanical properties in a transistor. Next, I discuss how the island of an SET functions like a quantum dot and then discuss the properties of a single tunnel junction. I then put all these components together and explain transport though an SET and the dependence of current flow on the bias and gate voltages. Finally, I describe how the SETs are used in the experiment to detect the charge of the phosphorus donor.

3.1 The Push Towards Single Electron Devices

The semiconductor transistor has been a very remarkable invention which is now an indispensable component of all modern electronics. Since its invention in the 1940's, the trend toward miniaturization of transistors has been very rapid, opening endless opportunities in the realm of information acquisition, processing, data storage and communication technologies [2]. As devices get smaller, faster and more densely packed, quantum effects become increasingly important for device operation. An example of such a device is the single-electron transistor (SET) which will be explored in great detail in the rest of this chapter. Electron transport in an SET is governed by the tunneling of electrons through an insulating barrier, a feat that cannot be

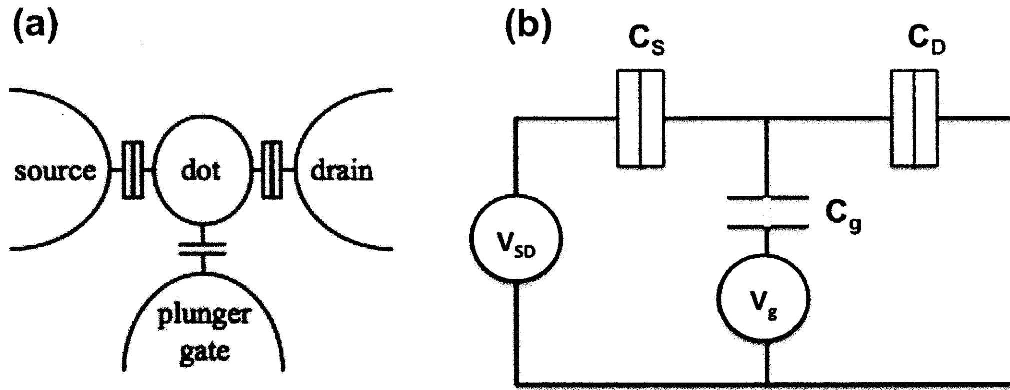

Figure 3-1: (a) Schematic of a single electron transistor. Taken from [10]. (b) illustrates the capacitance model for the SET.

explained classically.

The fabrication of tunnel junctions with increasingly smaller dimensions has made it possible to observe the quantum mechanical tunneling of a single electron through an insulating barrier. The SET consists of two tunnel junctions placed in series, forming an island between them. This island is a region containing localized electrons which functions like a quantum dot. It is coupled to a source and drain contact via tunnel junctions. The source and drain terminals connect the island to macroscopic current and voltage meters. We describe the SET using a circuit diagram as shown in Fig. 3-1. The functioning of an SET is governed by a combination of the quantum phenomenon of tunneling of an electron through a metal-insulator-metal junction and the Coulomb interactions on the island.

Fulton and Dolan were the first to demonstrate successful SETs in 1987 [7]. Since then SETs have been realized using a variety of fabrication methods and materials, including metallic, semiconducting, molecular and nanotube based devices. These different incarnations of the SET allow for different operational schemes and temperatures [20]. Typically, metallic based devices are operated in the milli-Kelvin temperature range, though there have also been devices that operate at room temperature [16, 17]. The operating temperature is an important parameter, as it partially defines the energy conditions which dictate electron tunneling events through the SET.

Current efforts have been focused on raising the operating temperature of the device in the hopes of overcoming one of the main drawbacks in the implementation of single-electron devices.

The most outstanding property of SETs is the possibility to switch the device from the insulating to the conducting state by adding only one electron to the gate electrode, whereas a common MOSFET needs about 1000 to 10,000 electrons [19]. This reduction in the number of electrons in a switching transition greatly reduces circuit power dissipation, raising the possibility of even higher levels of circuit integration [4].

SETs are extremely versatile in their applications. They can be used as very precise temperature sensors, magnetometers and electrometers [18]. They are already outperforming state-of-the-art conventional transistors by three orders of magnitude. Their charge sensitivity has been shown to be as low as a few $10^{-5}e/\sqrt{\text{Hz}}$, which means that a charge variation of $10^{-5}e$ can be detected in a measurement time of 1s where the precision improves as the square root of the measurement time [2].

3.2 The Quantum Dot

The SET consists of an island that connects a source and a drain via two tunnel junctions. This island is a quantum dot, with the defining feature that it contains localized electrons. In the past couple of decades, various structures have been fabricated to confine electrons to small volumes in both semiconductors and metals. A system of confined electrons will have discrete charge and electronic states . They are often called artificial atoms or quantum dots in order to reflect the importance of quantization phenomena on their properties [15, 14]. I now discuss the similarities and differences between the semiconductor and metallic quantum dots which can be seen in two limiting cases: (1) the case with a few electrons on the dot where the discrete level spacing is comparable to the charging energy and (2) the case with many electrons on the dot where the level spacing is much smaller than the charging energy [20]. I make some estimates of the energy scales involved using simple models

in order to get a feel for the physics.

Semiconducting Dots:

In semiconductors, electrons fill only a few levels of the conduction band. At the nanometer length scale, quantum dot devices have been fabricated where the electrons occupy discrete energy levels. These devices function like "artificial atoms," where the discrete excitation spectrum is analogous to atomic orbitals in atoms [13]. In these devices, the confinement of the electron can be modeled by a single particle in a box. This discreteness of levels is important because the level spacing is comparable to the chemical potential. The characteristic energy level spacing for a dot of typical radius R is given by:

$$\delta E \approx \frac{\hbar^2 \pi^2}{2m_e R^2}\left(\frac{m_e}{m^*}\right), \tag{3.1}$$

where m_e is the rest mass of the electron and m^* is the effective mass of the electron in the system [20].

We estimate the energy level spacing for a dot of size $R = 100nm$. In a semiconductor, the effective mass of an electron is approximately $m^* \approx 0.1m_e$, giving an estimate of the energy level spacing to be $\delta E \approx 0.4meV \approx 4K$. The number of electrons in a semiconducting dot is determined primarily by the dopant density that fill only the low lying states.

Metallic Dot:

Most metallic dots contain a large number of electrons, so Eq. 3.1 cannot be used to describe the energy spacing of the levels. The average level spacing at the Fermi energy is quite small and should be estimated using a density of states argument [14].

In our SETs, the island has dimensions much larger than the the lattice spacing of aluminum. Thus, we can approximate the number density of the dot as that of bulk aluminum. Assuming a 3 dimensional spherical dot, for a density $n = 18 \times 10^{22}/cm^3$, the number of electrons on the dot is on the order of $N = 4/3\pi R^3 \times n \approx 10^9$ [1]. Given the number of electrons, the picture is different from the semiconductor dot picture. With so many levels of the dot filled, we are no longer probing the bottom levels of a band. We can therefore view the metallic dot as a collection of a large

number of electrons filling up states up to the Fermi level ε_F. From this description, we estimate the energy level spacing (up to constant factors arising from geometry) from the inverse density of states $g(\varepsilon_F)$ since $\delta E = 1/g(\varepsilon_F)$, where the density of states is the number of states per energy [14]. Given that $\varepsilon_F = \hbar^2 k_F^2/(2m)$ and $k_F^3 = 3\pi^2 N/V$ we obtain $g(\varepsilon_F) = dN/d\varepsilon_F = 3N/(2\varepsilon_F)$. For a 3-D, $100nm$ Al dot with a Fermi energy $\varepsilon_F \approx 10eV$ this gives a level spacing of about $0.6 \times 10^{-5} meV$ which is much smaller than the estimate of a particle in a box. Thus we see that in a metallic quantum dot, the discrete energy spacings are very close together and cannot be resolved in most measurements.

Role of Coulomb Interactions in Quantum Dots:

If a quantum dot is relatively isolated electrically from its environment, it has a set of well defined charge states. Each successive charge state corresponds to an addition of one more electron to the dot. The charging energy E_C of a quantum dot is similar to the ionization energy of an atom, defined to be the energy required to add or remove a single electron to the dot. Because of the Coulomb repulsion between electrons, the energy between successive charge states can be very large.

The primary difference between metallic and semiconducting dots is that in the metallic dots the charging energy is much much larger than the level spacing whereas in the semiconducting dots they are comparable. In a metallic dot, given the large number of electrons, the level spacing is given by the inverse density of states. In semiconducting quantum dots, the energy level spacing can be modeled by the confinement of a few electrons in a box. However, what is important for the functioning of the SET is the possibility to measure charge quantization using either metal or semiconducting dots. Both types of dots share the fact that the Coulomb energy is an important energy scale and determines the quantum transport through the dot.

The SETs fabricated for this experiment are made of aluminum, consisting of islands with dimensions approximately 50nm by 50nm by 500nm and are best understood by the metallic quantum dot description.

It is also interesting to contrast the behavior of metallic dots *vs.* bulk metals. In the bulk of a metal, the electronic states are extended plane wave states resulting in

bands. The Coulomb interaction evaluated using these plane wave states are typically much smaller than the band width electron correlations can be neglected in bulk metals. Therefore it is possible to add an electron right at the Fermi energy E_F (at low temperatures) in the bulk metal. As electronic wave functions get localized on the quantum dots, the Coulomb interactions between these localized wave functions become significant. As a result the energy to add an extra electron on the metal dot becomes $E_F + E_C$, where E_C is the charging energy discussed above.

3.3 Charge Quantization for a Tunnel Junction

For a tunnel junction, i.e. two metallic electrodes separated by an insulating barrier, an electron at the Fermi energy of one of the electrodes can pass through the barrier to the other electrode, even though classically, the electron energy is too low to overcome this barrier. The charge Q transferred through the barrier is quantized by amount e, so the charge on the island is given by $Q = Ne$, where N is an integer. The number of electrons N is such that the energy of the entire circuit is minimized.

When a tunneling event occurs, the charge on the island changes by the quantized amount e. The associated change in the electrostatic potential of the island is E_C/e where the charging energy, $E_C = e^2/2C_J$ is expressed in terms of the capacitance of the junction C_J. In order for the thermal energy to not mask the Coulomb effects, we require that charging energy exceeds the temperature,

$$\frac{e^2}{2C_J} \gg k_B T. \tag{3.2}$$

This condition can be met by having tunnel junctions with a small capacitance which translates to having a small junction size, since for a parallel plate capacitor, $C = \epsilon A/d$.

Adding an additional electron to the island takes a time $\Delta t = R_t C_J$ given by the RC-time constant of the island. In order to resolve the charging energy $\Delta E_c = e^2/2C_J$, we must impose the condition that the system obeys the Heisenberg uncer-

tainty relation $\Delta E_c \Delta t > h/2$. Thus the tunneling resistance R_t of the quantum dot has to be larger than the quantum resistance,

$$R_t \gg \frac{h}{e^2}. \tag{3.3}$$

This criterion can be met by weakly coupling the island to the source and drain leads [10].

As an example, let us note that a junction with an area of about $0.1 \times 0.1 \mu m^2$ and a typical oxide layer thickness of $10\mathring{A}$ has a capacitance of about 10^{-15}F corresponding to a temperature of about 1K. For decreasing capacitance, which requires decreasing dimensions of the junction, this restriction for temperature becomes more relaxed.

3.4 Electron Transport Through an SET

Recall that an SET consists of an island coupled via tunnel junctions to a source and a drain and capacitively coupled to a gate. See Fig.. 3-1. Current flows through an SET when an individual electron tunnels through one of the tunnel junctions onto the island and then from the island through the other tunnel junction. A schematic of single electron tunneling is shown in Fig. 3-2. Thus the charge on the island is quantized and can only change in discrete units of e. When current flows through the SET, the charge on the island oscillates between N and $N + 1$ electrons.

The energy of the island with N electrons on it is given by

$$E_{dot}(N, V_g, V_{SD}) = \frac{(-en + Q_0)^2}{2C_\Sigma}. \tag{3.4}$$

with C_Σ being the total capacitance given by $C_\Sigma = C_S + C_D + C_g$ and $n = N - N_0$ where N is the number of electrons on the island and N_0 is the number of electrons at zero gate voltage and zero bias voltage. The continuous part of the excess charge, induced by the gate and bias voltages is given by

$$Q_0 = C_S V_S + C_D V_D + C_g V_g. \tag{3.5}$$

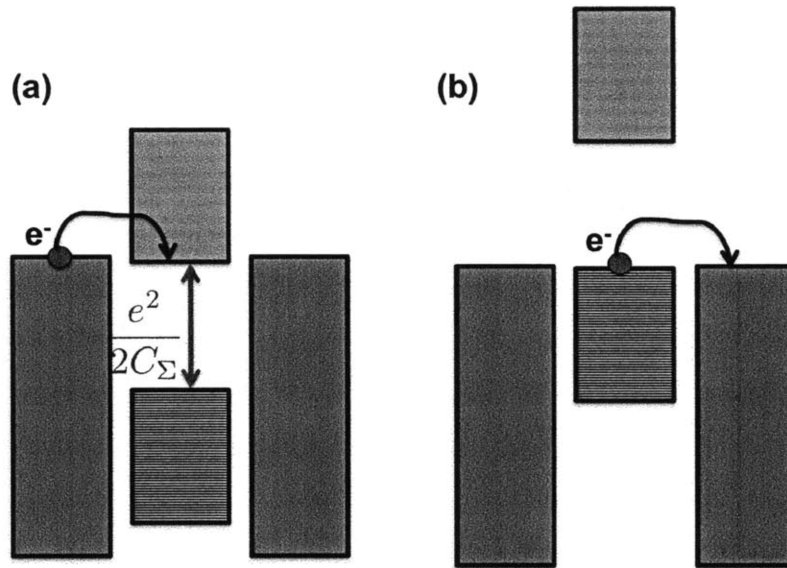

Figure 3-2: Schematic depicting how the tunneling of an individual electron through the source and drain tunnel junctions via the island induces a current flow through the SET. (a) shows the situation with N electrons on the dot and (b) shows the situation with N + 1 electrons on the dot. An additional electron on the island increases its energy by $Ec = e^2/2C_\Sigma$ or the potential by E_c/e. When current flows through the SET, the charge on the island oscillates between N and N + 1 electrons. (a) and (b) show the sequential tunneling process at the same gate voltage. Modified from [20].

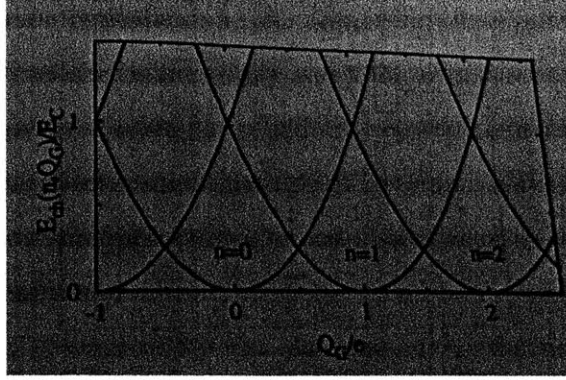

Figure 3-3: Energy parabolas showing the interplay between the continuous and discrete charges on the dot.Taken from [20].

For each value of n, the number of electrons on the dot, we get an energy parabola, plotted in Fig. 3-3. With a gate voltage it is possible to change the number of electrons on the dot. For a fixed value of Q_0 there is a minimum energy cost for the dot to change the electron number. While the tunneling of a single charge changes the electrostatic energy of the island by a discrete value, a voltage V_g applied to the gate can change energy of an island in a continuous manner. At $Q_0/e = \pm 1/2$ integer values two different charge states with different numbers of electrons become degenerate. At these values of the gate voltage, charges leads to conductance dI/dV oscillations as a function of gate voltage, also known as Coulomb oscillations.

The energy required to add an additional electron to the island is known as the charging energy. The charging energy is given by

$$E_C = \frac{e^2}{2C_\Sigma}. \tag{3.6}$$

To be able to resolve the charging energy of an SET is very similar to that of an individual tunnel junction, and is given by

$$E_C = \frac{e^2}{2C_\Sigma} \gg k_B T. \tag{3.7}$$

In this case C_Σ is the total capacitive coupling to the environment, which for an SET is given in terms of the source, drain and gate capacitances: $C_\Sigma = C_S + C_D + C_g$.

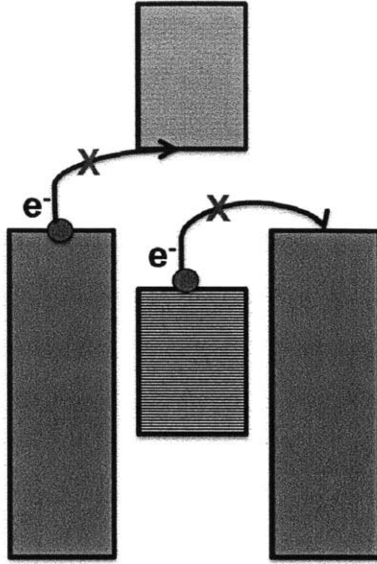

Figure 3-4: Schematic of the Coulomb blockade regime where the electron is unable to tunnel onto or off the island because it cannot overcome the charging energy of the island. In this case, no current flows through the SET.

Tuning the gate voltage V_g changes the energy of the island continuously, moving it up or down with respect to the source and drain, but not affecting the charging energy. If the electrons cannot overcome the charging energy of the island, no current flows through the SET. When electron transport is blocked, the device is said to be in the Coulomb blockade regime. This is shown schematically in Fig. 3-4.

We now calculate the dependence of the Coulomb oscillations and Coulomb blockade on parameters such as the gate voltage and bias voltage. Based on the circuit model for the SET, the voltage of the island is given by

$$V_{dot} = \frac{Q_0}{C_\Sigma} = \frac{C_S V_S + C_D V_D + C_g V_g}{C_S + C_D + C_g} \tag{3.8}$$

For no bias voltage, we can shift the energy of the island, V, by applying a small gate voltage. Applying a bias voltage to the SET shifts the chemical potential of the source relative to the drain. We set the drain voltage to be our reference and measure all voltages from that point. Changing the bias voltage also changes the energy of the island since the island is weakly coupled to the source and drain. At

zero temperature, current flows through the SET when the number of available states on the island in the energy between V_S and V_D is non-zero.

First, for zero bias voltage, as we sweep the gate voltage, the conductance oscillates between zero (Coulomb blockade) and non-zero (no Coulomb blockade) as illustrated in Fig. 3-5. In the case of zero conductance, the number of electrons N on the island is fixed. At the conductance maximum, this number oscillates between N and $N+1$. We now derive the period of oscillations in gate voltage corresponding to conducting resonances through the SET. The energy of an island with N electrons is given by

$$E_{dot}(N) = \frac{(-en + Q_0)^2}{2C_\Sigma}. \tag{3.9}$$

Therefore, the energy difference between an island with $N + 1$ electrons versus N electrons is given by

$$E_{dot}(N+1) - E_{dot}(N) = (n - 1/2)\frac{e^2}{C_\Sigma} - e\frac{Q_0}{C_\Sigma}. \tag{3.10}$$

For zero bias voltage, $V_S = V_D = 0$,

$$E_{dot}(N+1) - E_{dot}(N) = (n - 1/2)\frac{e^2}{C_\Sigma} - e\frac{C_g V_g}{C_\Sigma}. \tag{3.11}$$

As we saw in Fig. 3-3, At the intersection points of the $E(N)$ and $E(N+1)$ parabolas, we get a conductance peak through the SET. In order to find the gate voltage when $E(N+1) = E(N)$, we set Eq. 3.11 to zero, giving:

$$V_g(n) = \frac{(n - 1/2)e}{C_g}. \tag{3.12}$$

Thus, for zero bias voltage, in order to find the period of oscillations in gate voltage, ΔV_g, corresponding to a change of one electron, is given by

$$\Delta V_g = V_g(n+1) - V_g(n) = \frac{e}{C_g}. \tag{3.13}$$

A 2D plot of the conductance as the bias voltage and gate voltage are swept

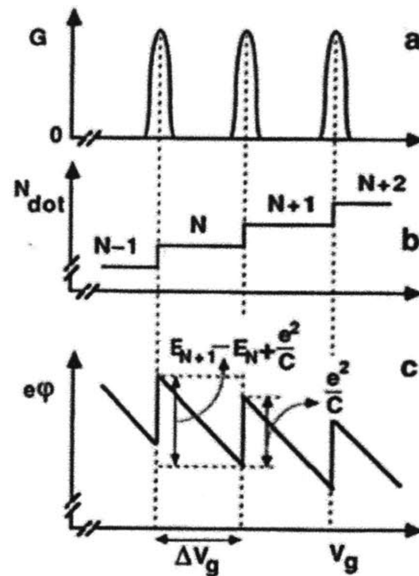

Figure 3-5: Schematic representation of conductance through a quantum dot as a function of gate voltage with a fixed bias voltage of $V_{SD} = 0$. (a) illustrates the conductance, (b) shows the number of electrons on the dot and (c) shows the electrostatic energy of the dot. Between Coulomb oscillations, the number of electrons on the dot is fixed corresponding to the Coulomb blockage regime. At a conductance resonance, the number of electrons on the dot oscillates by one, and the electrostatic energy oscillates by e^2/C_Σ. Taken from [6].

shows the characteristic Coulomb diamonds a schematic of which can be seen in in Fig. 3-7. The height of the diamond is proportional to the charging energy and given by $2 * e/2C_\Sigma$ and the width is given by $\Delta V_g = e/C_g$. As per the chemical potential picture shown in Fig. 3-6, the slopes of the Coulomb diamond are defined by $V_D = V_{dot}$ and $V_S = V_{dot}$. From these equations it is possible to derive the explicit relationship between the bias voltage and the gate voltage in terms of the various capacitances in the system.

In order to determine the slopes of the Coulomb diamonds, i.e. the regions of current flow, we apply a fixed positive gate voltage V_g to the SET, and adjust the bias voltage such the energies of the source or drain is equal to the energy of the island.

For a forward biased SET, current will flow when $V_S = V_{dot}$ as shown in Fig. 3-6 (a). This condition gives rise to the equation

$$V_S = \frac{C_S V_S + C_D V_D + C_g V_g}{C_\Sigma}. \tag{3.14}$$

Setting $V_D = 0$ and solving for V_S/V_g, we get

$$\frac{V_S}{V_g} = \frac{C_g}{C_\Sigma - C_S} = \frac{C_g}{C_g + C_D}. \tag{3.15}$$

For a reversed biased SET, we want the condition, $V_D = V_{dot}$ as shown in Fig. 3-6 (b). Since V_D is our reference, we have

$$0 = \frac{C_S V_S + C_D V_D + C_g V_g}{C_\Sigma}. \tag{3.16}$$

Solving for V_S/V_g, we get

$$\frac{V_S}{V_g} = -\frac{C_g}{C_S}. \tag{3.17}$$

Thus Eq. 3.15 and Eq. 3.17 give us the slopes of the Coulomb diamonds. We see that Eq. 3.15 and Eq. 3.17 are not symmetric under the exchange of C_S and C_D. This is due to the fact that the we set the drain as the reference and apply the bias voltage

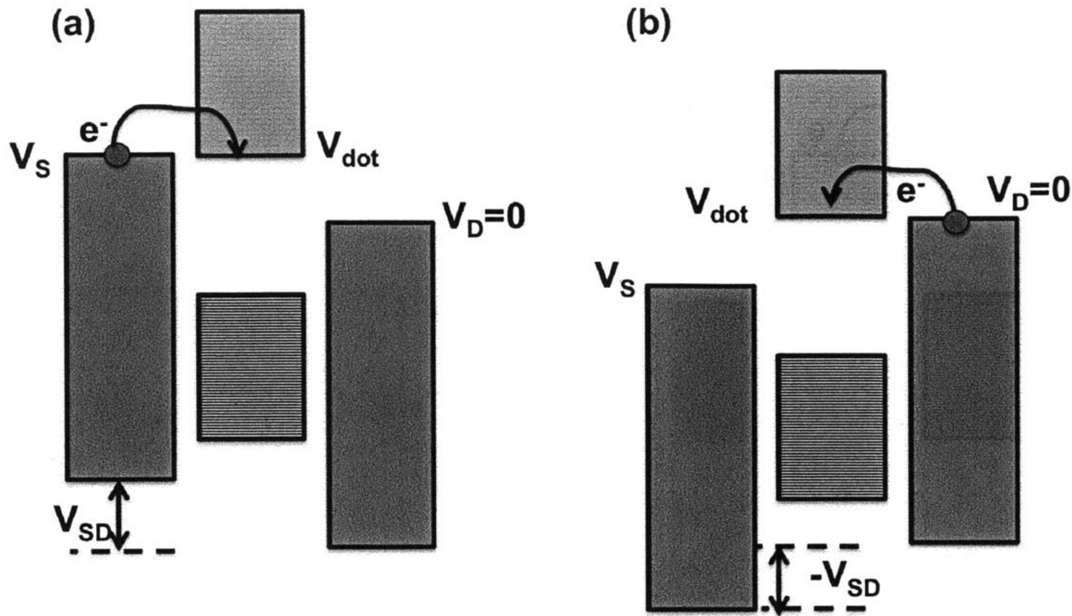

Figure 3-6: Schematic representation of energy of island compared to that of the source and drain during current flow through an SET. For a positive gate voltage, (a) shows the onset of current flow for a forward biased SET and (b) shows the onset of current flow for a reverse biased SET.

solely to the source. We perform the calculation for this case because in our transport experiments, we ground the drain and apply a bias voltage to the source. If we were to apply half of the bias voltage to the source and half to the drain, then the slopes of the Coulomb diamonds would be equal and opposite. However, the capacitances measured from the slopes should be the same, regardless of how the bias voltage is divided between the source and the drain.

3.5 Role of SETs in P doped Si experiment

For the experiment, we make the island and the source and drain leads of the SET from Aluminum. The SETs are fabricated directly on the P doped Si sample. This sample is placed in a cryostat in order to satisfy the condition that the charging energy of the SET is much greater than the temperature. The sample is irradiated with laser light tuned to a specific frequency. We then use the SET to electrically detect the

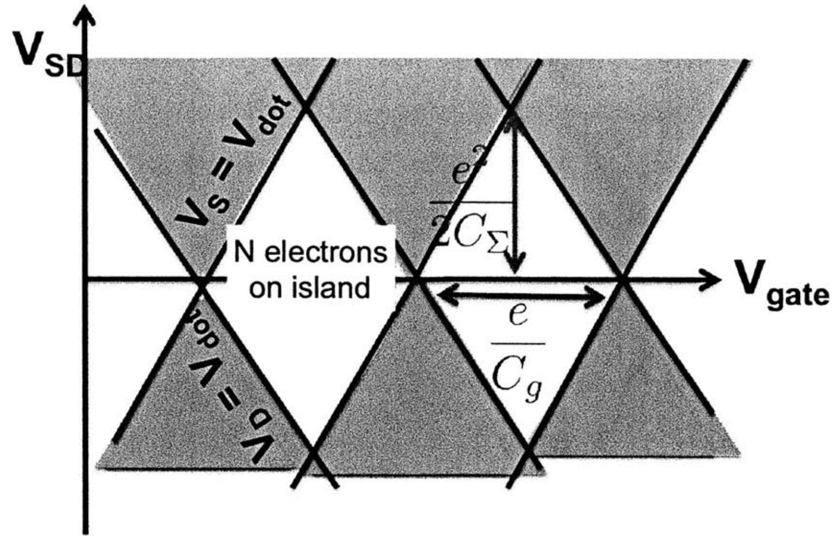

Figure 3-7: Schematic of the Coulomb blockade diamonds. Current flows in the gray triangular shaped regions. The white regions correspond to a gap in current flow with a fixed number of electrons on the island. Modified from [10].

charge of the P donor. If the P is ionized via the Auger process, the presence of the P^+ ion will shift the electrochemical potential of the island, with its effects similar to that of applying a gate voltage to the SET. From the above discussion, we see that this results in a sharp peak in the current through the SET, which can ultimately be used for single shot readout and thus for a measurement of the spin state of the electron. The next chapter of this thesis discusses the details of the fabrication of these SETs, and the following chapter presents measurements of the charging energy and charge sensitivity of the SETs that are to be used in the experiment.

Chapter 4

SET Fabrication

In this chapter, I discuss the fabrication procedures used to pattern SETs on a silicon substrate. First, photolithography is used to pattern ohmic contacts onto our sample. The gates allow us to make electrical contact between external voltage sources and the leads of the SET. Two stages of photolithography are involved in order to ensure good electrical contact at both ends. After the ohmic contacts are patterned on the sample, we write the leads and island of the SET using electron beam lithography. Fig. 4-1 is a schematic of the various features written during the entire fabrication process for a single SET. Since we are spatially trying to probe various P donors in Si, we pattern several SETs at a time in order to improve our yield. We write sets of 15 SETs on a mesa as shown in Fig. 4-2.

In order to utilize SETs for sensitive charge measurement experiments, it is necessary to have a reliable and reproducible fabrication procedure for these SETs. My starting point was a fabrication recipe for SETs designed by other Yacoby Group members. This recipe produced SETs on a GaAs substrate with a charging energy of ~2K. The goal of my experiment is to have SETs on Si that can operate in a helium cryostat that goes down to temperatures of ~2K. However, the condition $E_c >> k_B T$ requires that my SETs have a charging energy much larger than 2K. Through considerable experimentation, I modified the old recipe to create SETs with a charging energy of $\sim$ 9.5K which can be operated in the 2K regime. This necessitated minimizing the tunnel junction area through optimized lithography and

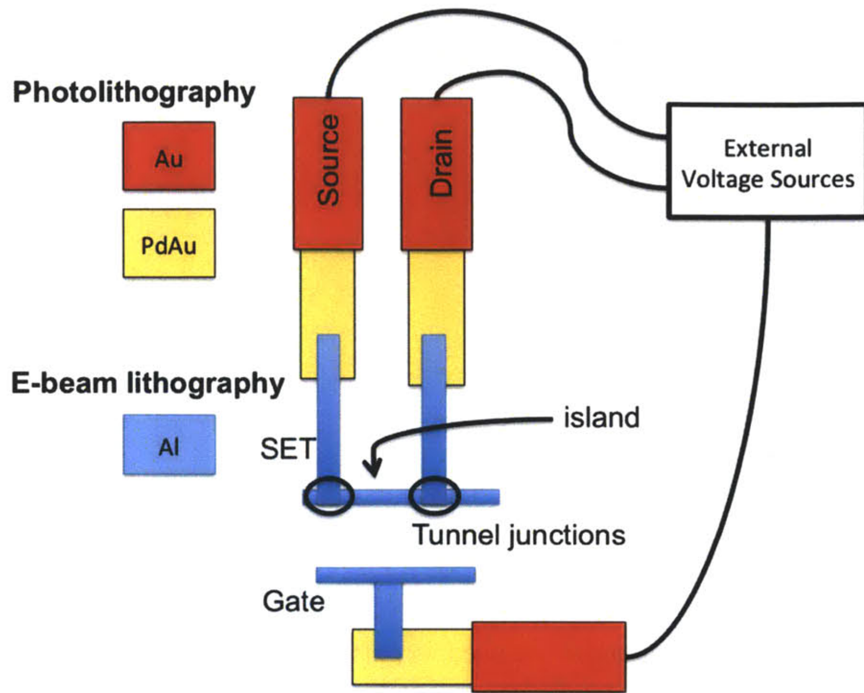

Figure 4-1: Schematic of an SET. The ohmic contacts are made using photolithography and the SET pattern is made using e-beam lithography.

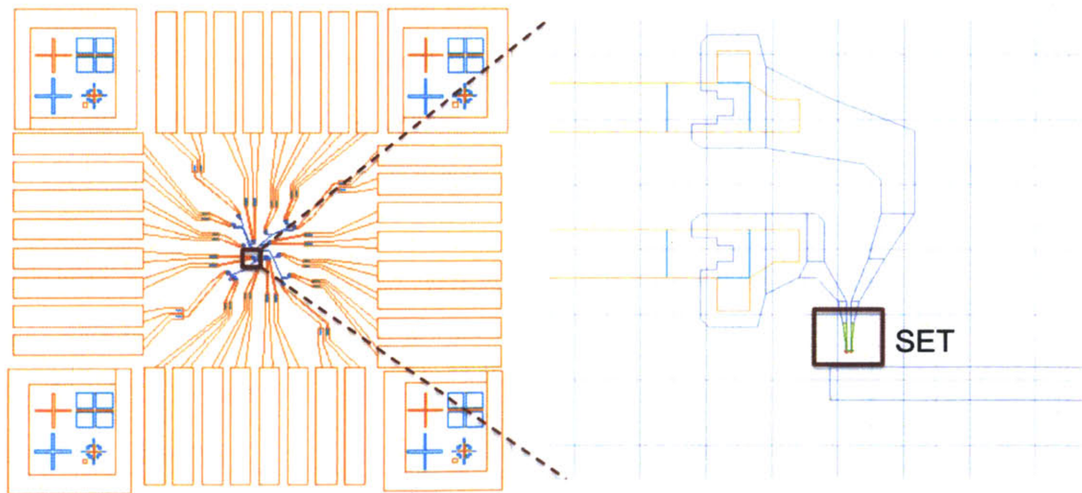

Figure 4-2: Picture of TurboCAD file of one mesa containing 15 SETs capacitively coupled to gates. The outer orange rectangles are the ohmic contacts to which we wire bond in order to make electrical contact. They also connect to the dark blue features in the middle of the mesa. These dark blue features are the gates and SETs. The light blue on the outside are alignment markers sued to align all features on the mesa. On the right, a zoomed in picture of one SET is shown.

evaporation procedures. I was able to reduce the area of the tunnel junctions from 45nm by 45nm to 30nm by 30nm.

4.1 Ohmic Contacts

The ohmic contacts, with features ranging from millimeters to micrometers, are patterned on the substrate using photolithography. These gates are used to make electrical contact between the SET leads and the external voltage sources. In photolithography procedures, first resist is spun onto a sample. A mask with the optical gate pattern is exposed with UV light, transferring the pattern from the mask to the resist on the sample. The sample is then developed, removing resist in the areas that were exposed. Metal is then deposited over the entire surface of the wafer. The remaining resist is removed in a solvent bath, lifting off the metal that was deposited on top of the resist, and leaving metal only in the areas where the photoresist was previously exposed.

Resist Spinning and Exposure: A bilayer resist scheme is used in order to create an undercut that aids in the liftoff process of the metal. We first spin a layer of LOR resist which is very sensitive to exposure. Above this we spin a thin layer of Shipley S1805 photoresist. This bilayer photoresist stack is exposed to high intensity UV light, transferring a pattern from the mask onto the resist. On the mask aligner MA6, we use hard contact and expose the sample for 4.0 seconds. The sample is then developed, removing resist only in areas that were exposed. The desired pattern is transferred to the S1805, and the LOR layer acts as a spacer between the S1805 mask and the wafer surface.

Evaporation and Liftoff: Thermal evaporation is used to deposit the desired metals over the entire wafer surface. The wafer is then soaked in a PG Remover at 60°C, lifting off the metal deposited on top of the resist and leaving metal only in areas where there was no photoresist. Due to the bilayer resist scheme, the metal on the surface of the wafer does not connect to the metal that is on top of the resist, ensuring good liftoff. This process is illustrated in Fig. 4-3.

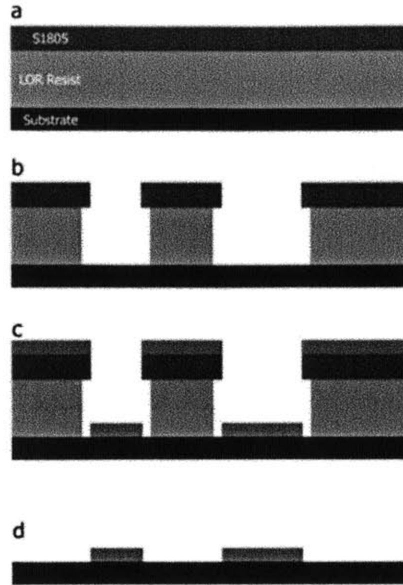

Figure 4-3: Schematic representation of photolithography procedure. (a) resist bilayer on substrate (b) after exposure and development (c) metal deposition (red) (d) after resist removal. Taken from [9].

In order to ensure good electrical contact for measurement, the connection to the SETs and the contact to the electrical leads must both be good, with low contact resistance at the interface. For this reason, these ohmic contacts have two different components - the small gates form a Palladium-Gold (PdAu) contact to the SET leads, while the large gates are Gold (Au) pads to which we can wire bond electrical contacts.

This photolithography is repeated twice, first to create the contact to the SET leads and then to form the gold pads. The first time, we use a mask that has both the large and small gates and deposit 75 Å layer of PdAu over a 50 Å Ti sticking layer. The second time, we align a mask with only the large gates to the already patterned and evaporated large+small gates. This time we evaporate a 200 Å Ti sticking layer and above it a 1000 Å Au layer. In this fashion, we are able to have different metals contact the different components of our system, as desired.

Previous Recipe: The original recipe to make ohmic contacts on GaAs called for using an image reversal technique. This technique uses a negative tone resist to

create an undercut profile. Instead of exposing the feature where the metal is desired, the areas around the feature are exposed However, this process is highly sensitive to a certain baking temperature and we did not get consistent results when this process was transferred to a silicon substrate.

We therefore decided to use positive tone resist. In order to change photolithography recipes, we had to order a suitable positive mask. Additionally, only four to six mesas were patterned at a time on a small GaAs sample. We designed a 5 inch mask suitable for a 4 inch wafer. The mask contained a 10 by 10 array of mesas; 100 mesas total. Two mask were made, one with both the small and large gates and one with just the large gates. Future mask design should include alignment and orientation markers outside the array of mesas to aid in the alignment of the large gates with the small gates.

The natural SiO2 layer on top of any silicon sample makes it hard for metals evaporated on a Si substrate to stick to the surface. We encountered difficulty in getting the PdAu to stick directly to silicon substrate so we had to deposit a Ti sticking layer first, which was not the case for our old GaAs.

4.2 Electron Beam Lithography

In electron beam lithography, a beam of electron rasters a pattern across a substrate coated with a sensitive resist layer. The beam reacts with the resist, exposing it. Once developed, the exposed resist is removed, creating a mask through the substrate.

TurboCAD is used to make the file which contains the pattern to be written using e-beam. It is easy to modify this pattern, making it possible to write patterns with many different leg and island widths in order to see which ones would have the smallest tunnel junctions and thus the highest charging energy. An example of a single SET is shown in Fig. 4-4.

To optimize pattern resolution, it is necessary to vary beam parameters affecting the sample, including current and dosage. Usually a trial and error process guided by the known material parameters is required to optimize these parameters so as

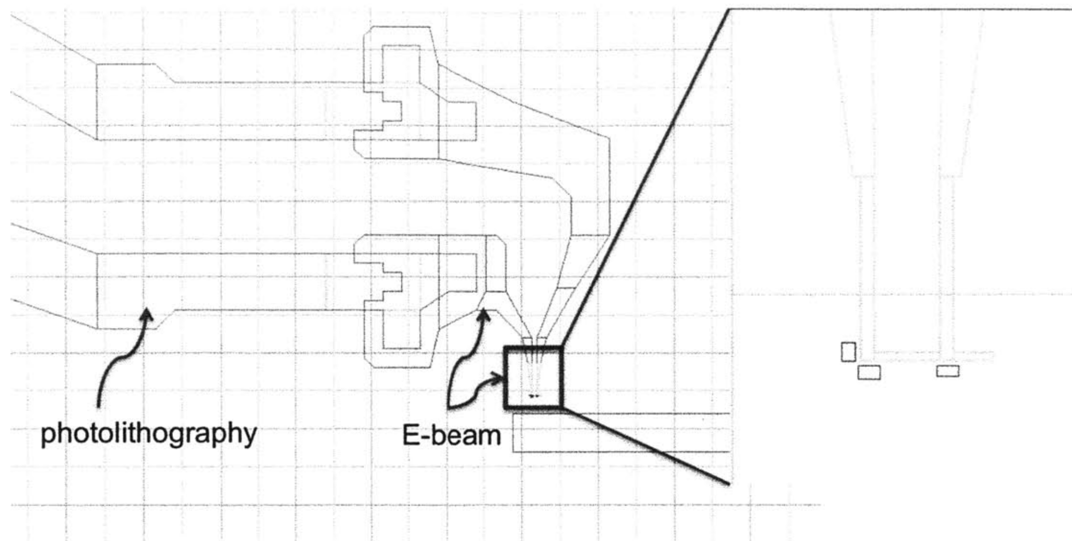

Figure 4-4: Example image of the TurboCAD file in which we can specify widths of SET island and legs.

to not over or underexpose the sample. A major factor affecting lithographically produced patterns is the proximity effect. As electrons penetrate the resist, they undergo many small angle scattering events. This can tend to broaden the beam on the resist, causing the feature to receive unwanted additional dosage. Additionally, focus, astigmatism and aperture settings all need to be optimized in order to achieve desirable linewidths for each pattern writing session.

Resist: We pattern our SETs using e-beam lithography with a bilayer resist scheme. The previous SET recipe produced SETs with 50nm by 50nm tunnel junctions. The two layers of resist were a copolymer layer of MMA (8.5) MMA EL$\sim$ 6% followed by 950 PMMA A4. In order to decrease the size of the tunnel junctions, we experimented with thinner resists which would allow us to write smaller features. In our modified recipe, the first (bottom) layer is a sensitive copolymer, MMA (8.5) MMA EL 3%, which provides an undercut to aid in the lift off process. The second (top) layer is a PMMA A2. Both layers are spun at 5000rpm for 40 seconds and then baked at 180 C for 5 minutes. Above this, we spin a thin layer of high conductivity e-spacer, in order to solve positional errors during the e-beam write due to charging effects.

Exposure Parameters: We write the SET features using a beam current (rate of electron charge deposition) of 50pA. The pattern is written with a resolution of 60,000 dots in a 75μm by 75 μm area. During each write session, we must optimize the aperture settings as well as the focus and stigmation for the desired beam current. It is also necessary to check that the height of the sample and thus the focus of the beam does not vary too much in different areas of the sample. After adjusting the focus and stigmation, we must align the e-beam pattern to the already present photolithography pattern of the gates on the sample. The SETs are exposed with a dose of 1750 μC/cm^2 corresponding to a dose time of 0.55 μs/dot. This dose time depends on the beam current with which the features are being written as well as the intensity of the beam.

4.3 Shadow Evaporation

Metal is deposited on a substrate using thermal evaporation. The evaporation procedure for the photolithography step is fairly standard. Now I describe the evaporation process used to make tunnel junctions that is performed after e-beam lithography.

After e-beam exposure on a bilayer resist coated wafer, the substrate is developed, removing the exposed resist. This creates an undercut resist profile where the top resist layer is suspended over the bottom. Separate layers of metal are deposited in an evaporator at oblique angles, a process known as shadow evaporation, in order to make small area tunnel junctions [3]. We use the evaporator in the Yacoby Group in which the sample can be mounted on a stage where we can control the polar and azimuthal angles. To optimize the dimensions of our tunnel junctions, it is necessary to determine the most advantageous angles at which to perform the evaporation.

Our shadow evaporation procedure is such that during the first evaporation we wish to deposit metal only into the island of the SET. The deposited metal is then oxidized to form the tunnel barrier. The second evaporation is meant to fill in the legs of the SET and form tunnel junctions at the overlapping points between the legs and the island. A schematic is shown in Fig. 4-5.

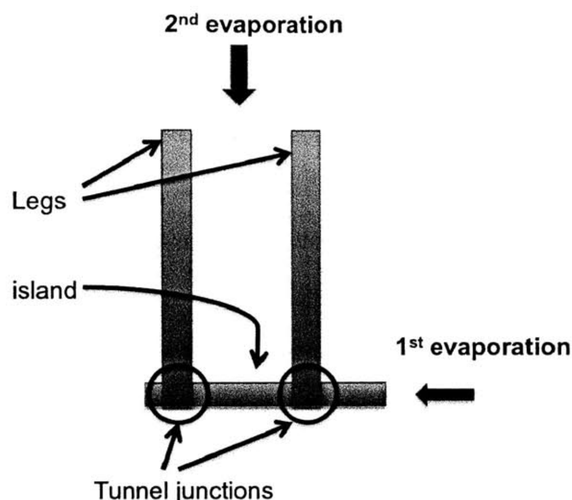

Figure 4-5: Schematic of an SET with the legs connected via tunnel junctions to the island. Explains the evaporation procedure.

During the first evaporation, we wish to evaporate at a polar angle larger than the critical angle such that we can choose to only deposit metal on the island of the SET and no metal is deposited in the legs. Fig. 4-6 shows a schematic of the cross section of the resist profile for the leg of an SET. The mask consists of the copolymer layer of resist with thickness δ_1 and the resist layer with the desired pattern of thickness δ_2. The size of the exposed region, labeled by w, corresponds to the width of the SET leg. From basic trigonometry we see that the critical angle depends only on the width of the feature and the thickness of the suspended resist layer, with

$$\theta_C = \arctan\left(\frac{w}{\delta_2}\right). \tag{4.1}$$

First the island is created by evaporation of Aluminum at a polar angle of $\theta = 45°$ and an azimuthal direction parallel to the island trench, say $\phi = 0°$. At this evaporation angle, 112 Å of Al is deposited. The tunnel barrier is then formed by oxidizing a thin layer of the Aluminum deposited on the island. The island is exposed to dry air at a pressure of 2.6 torr for 5.5 minutes, creating an 1nm thick insulating oxide layer. The sample is then rotated by an azimuthal angle of $\phi = 90°$ such that the legs are now parallel to the evaporation direction. To form the legs, 162 Å of Al

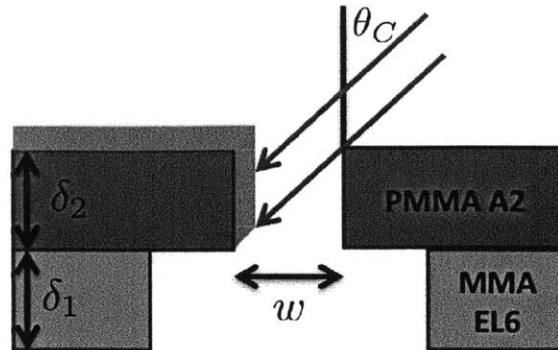

Figure 4-6: Schematic showing the first evaporation of shadow evaporation procedure for an SET leg. At this stage of the evaporation we only want to deposit metal into the island and not into the legs. For this to occur, the angle of evaporation must be at least the critical angle.

is deposited. See Fig. 4-5 and Fig. 4-6.

The resistance and capacitance of the tunnel junction will depend on the thickness of the oxide, and thus the amount of oxidation time, as well as the overlap area between evaporation steps.

The liftoff is carried out using by immersing the sample in boiling acetone.

4.4 Dose Test

In order to calibrate a new e-beam recipe, we must first perform a dose test to determine the optimal dose at which the pattern should be written. The dose, charge per surface area measured in $\mu C/cm^2$, is analogous to the exposure time. A dose test involves writing the SET (without the leads) at various doses in order to determine the optimal dose. This dose test pattern is written twice on one sample which is then cleaved. On one of the samples, we perform a standard, polar angle $\theta = 0°$ evaporation, while the other sample we evaporate using the shadow evaporation process described above. An example of a dose test pattern is shown in Fig. 4-7. This pattern is written at different doses, giving us the ability to see which dose and island size works best.

We then image the SETs using a Scanning Electron Microscope (SEM), looking

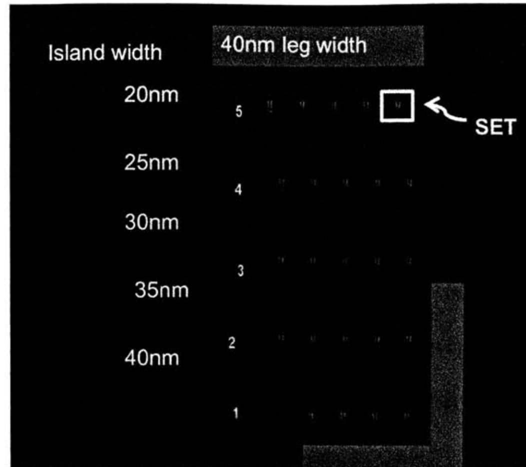

Figure 4-7: SEM image of a dose test pattern that is repeated at several different doses in order to determine optimal dose.

for the dose which leads to the smallest feature size that is completely formed and closest to the widths specified in the pattern file. Overexposed images tend to be wider than specified, with features that are not as sharp.

From such a dose test, we were able to determine that the dose time of 0.55 μs/dot for the SETs works best since the SET island widths that most closely matched the widths of the file. For higher doses times (0.70 and 0.82 μs/dot), islands still looked good, but were much wider than expected width based on file. An example of this is shown in Fig. 4-8

4.5 Resist Thickness and Angle Determination

In order to figure out the optimal polar angle at which to perform our shadow evaporation, it is necessary to first determine the thickness of our resist. We measure the resist thicknesses in two ways: using a Vecco Optical Profilometer and using an SEM. We spin a layer of resist on a silicon chip and use the SEM to expose a square region of the resist. The profilometer has a tip which quantitatively measures the surface profile. As the tip scans across the exposed region of our sample, we are able to obtain a measure of the resist thickness. To measure the resist thickness using an SEM, we spin a layer of resist on a chip and expose a cross using e-beam lithography.

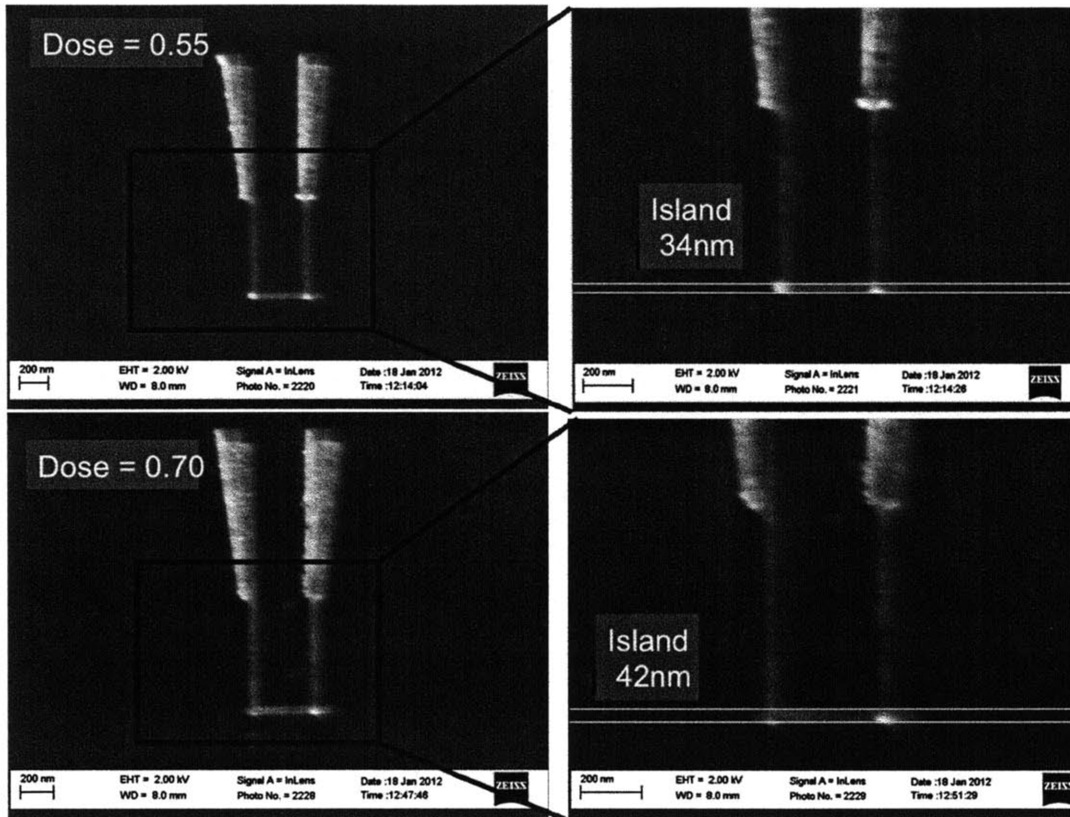

Figure 4-8: SEM image illustrating the optimal results from the dose test. An angle evaporation with a polar angle of 45° was performed. We compare widths measured in the SEM to the ones specified by the files used for the e-beam. In the write file, the SET islands had a width of 30nm. For a dose time of $0.55\mu s/\text{dot}$, islands were measured using an SEM to have a width of 34nm. For a dose time of $0.70\mu s/\text{dot}$, islands were measured using an SEM to have a width of 42nm.

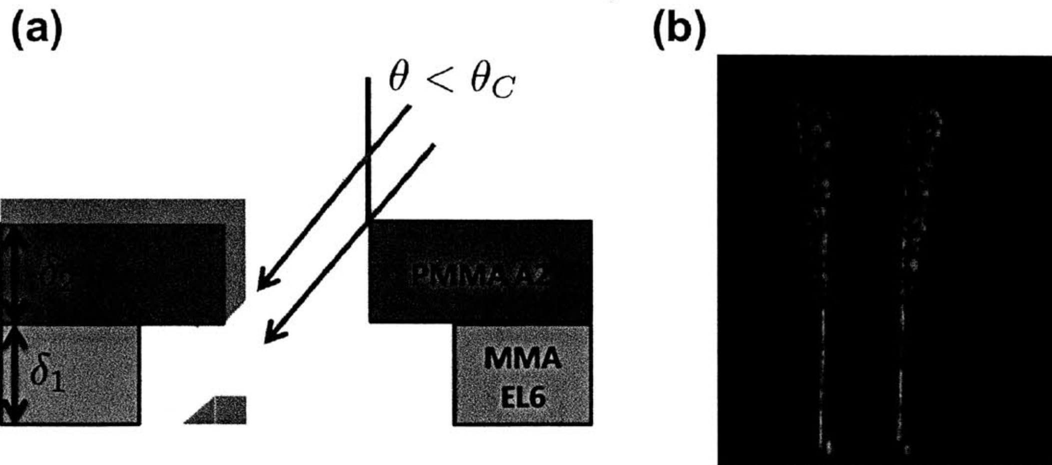

Figure 4-9: Shadow Evaporation less than critical angle. (a) shows a schematic of the SET legs during the first evaporation. The first evaporation is meant to only deposit metal in the island, but here (for angles less than the critical angle) we see that some metal is deposited in the legs as well. This leads to the shorting of the island to the legs as can be seen in the SEM image of the SET (b).

We place the sample of a 45 degree sample holder and measure the shadow seen at a 45 degree tilt due to the thickness of the resist.

We find the MMA EL3 layer to be ~50nm and the PMMA A2 to be ~50nm as well. During the first evaporation we wish to only deposit metal in the island and not the legs. The SET legs in our file are at most $w = 40$nm wide, which gives a critical angle of 38°. To be safe, since the resist profiles are not necessarily sharp rectangles, we perform our evaporations at a polar angle of 45°.

Fig. 4-9 shows SETs that were evaporated at a polar angle $\theta = 35°$, an angle less than the critical angle. The first evaporation from the right seemed to come in at too steep an angle depositing some metal into the legs even though our intention was to only deposit metal in the island. The extra metal deposited in the legs due to not enough shadowing, leads to the doubling of the legs, causing several of the SETs to be shorted. We also have trouble with liftoff, shown in Fig. 4-10, if there is metal stuck to the walls of the undercut layer. This can occur if the incorrect evaporation angle is used.

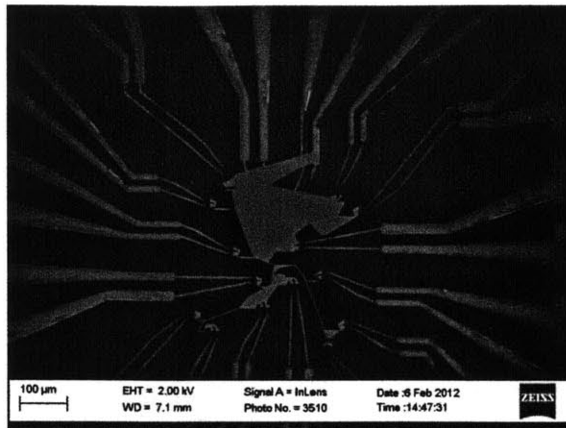

Figure 4-10: A mesa with 15 SETs where the liftoff was not successful. Most of the e-beam pattern is still covered in metal from the evaporation.

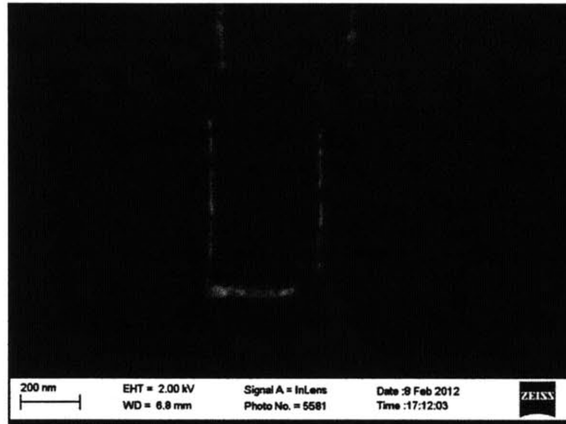

Figure 4-11: SEM image of an SET written without having optimal focus and stigmation. Island and legs are not continuous.

4.6 Focus and Alignment Problems

Fig. 4-11 shows an SET written without having optimal focus and stigmatic. The island and legs are not continuous and the tunnel junctions have not been formed.

Fig. 4-12 illustrates good versus bad alignment. In order to electrically test these SETs we must have good photolithography and good alignment of the SET pattern to the photolithography pattern. In the case of bad alignment, the SET legs are shorted together rendering any electrical testing of these SETs useless.

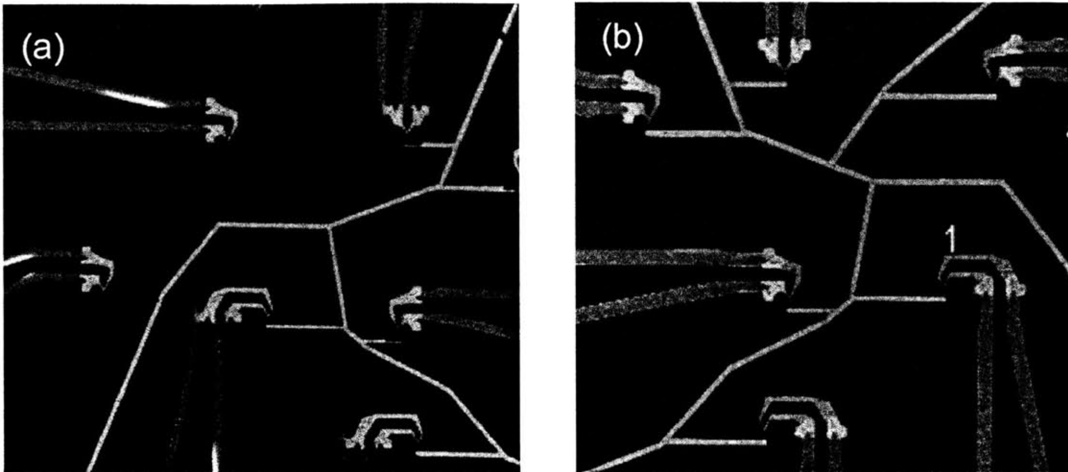

Figure 4-12: SEM image showing the comparison between (a) bad alignment and (b)good alignment of the e-beam step to the photolithography one. In the case of (a) we would not be able to make electrical contact to the SET and so would not be able to test the SETs.

4.7 Successful SETs

After optimizing all these different parameters, we had several successes of SETs. Fig. 4-13 shows the smallest island and leg widths that we have been able to achieve using e-beam lithography. We were able to obtain features as small as 30nm by 30nm tunnel junctions. However, the ohmic contacts on this sample did not come out well, as shown in the SEM image of the mesa in Fig. 4-14. Therefore we were not able to make electrical contact to the SETs. Thus we were not able to measure the electric characteristics of these SETs.

Fig. 4-15 shows the device that has islands 35nm wide and legs 40nm wide. Unlike the previous sample, the ohmic contacts were well aligned to the SETs, and we were able to make good electrical contacts. Therefore, we measured these SETs in a dilution refrigerator. The SET characterization measurements are discussed in the following chapter.

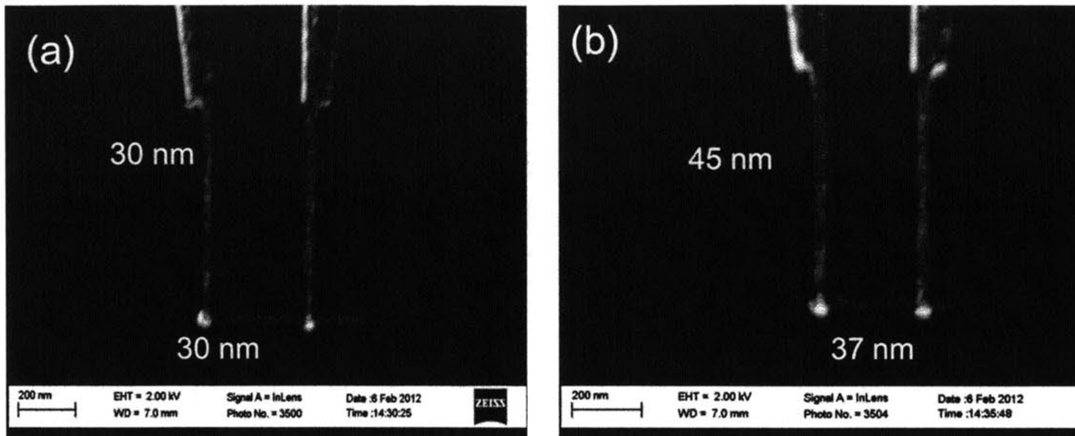

Figure 4-13: Compare file parameters to measured feature size. (a) File parameters for the SET are 25nm wide island and 30nm wide legs. On the SEM, we measure 30nm wide islands and 30nm wide legs. (b) File parameters are 35nm wide island and45 nm wide legs. On the SEM, we measure 37nm wide islands and 45nm wide legs.

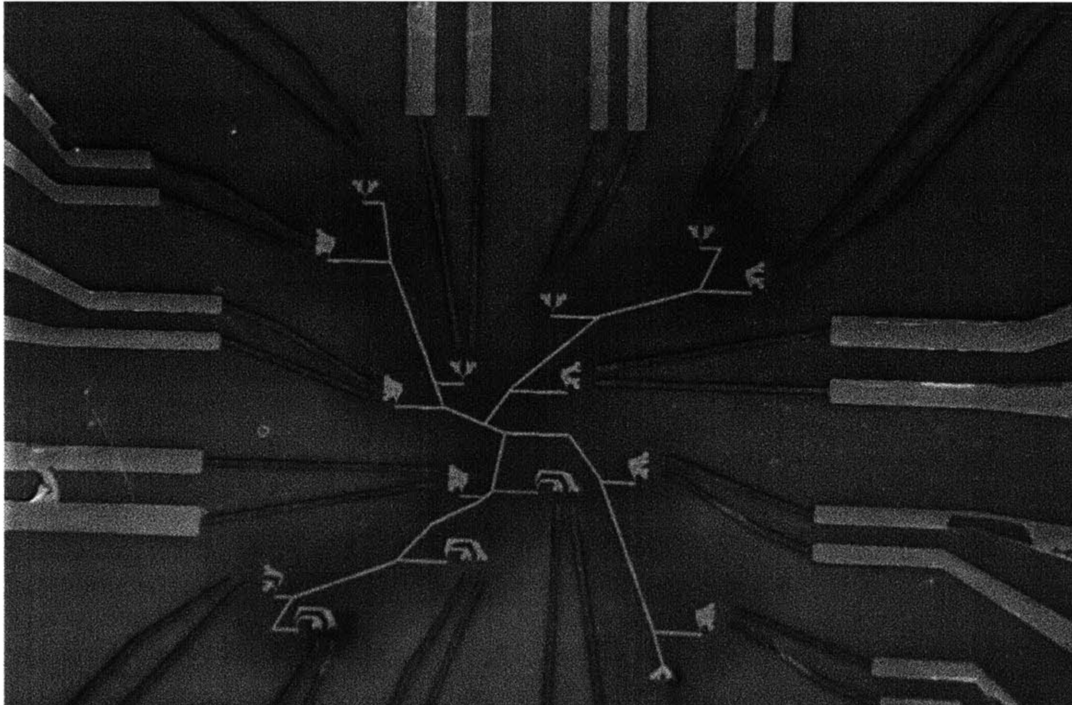

Figure 4-14: The SETs on this mesa were very good, but the small gates made with photolithography did not come out. Thus we were not able to make electrical contact to the SETs.

Figure 4-15: SEM image of a mesa containing SETs with 35nm wide islands and 40nm wide legs. This sample had good electrical contact of the pads to the SET. We characterize these SETs in a dilution refrigerator.

Chapter 5

SET Characterization

Transport measurements are used to characterize the SETs. In this chapter, I first describe preliminary measurements of the SET resistance. By measuring the resistance and conductivity for different applied voltages or currents, we can determine the functioning of the SET devices. Next, I describe the measurements performed in a dilution refrigerator. We measure Coulomb oscillations and Coulomb blockade diamonds by sweeping the bias and gate voltages. From these measurements we can obtain values for several parameters of the SET as well as determine the charge sensitivity of the device. The charge sensitivity is the charge variation that can be detected in a certain measurement time window where the precision improves as the square root of the measurement time.

5.1 Preliminary Measurements

We perform some preliminary resistance measurements at liquid helium temperatures of 4K. Measuring the resistance of the SET is the simplest way to determine whether the SETs have functioning tunnel junctions or are defunct either due to shorted leads or broken leads.

We mount the sample onto a chip carrier and wire bond the ohmic contacts on the chip to pins on the chip carrier. The chip carrier is then inserted into a Helium dewar. We determine the resistance of the SETs from the characteristic current-

voltage curves of the device measured using a parameter analyzer. We apply a DC bias voltage between the source and drain of the SET while grounding the gate. By sweeping the bias voltage and measuring the current through the SET, we can obtain an I-V curve for the device. For the old SET recipe, resistances of about 300kOhm were measured whereas the resistances of new SETs fall in the range of 2-5MOhms. In our new SET recipe, we have decreased the area of the tunnel junctions significantly, so we expect the resistance of the device to increase.

At 4K we tried to measure Coulomb Oscillations but were not able to resolve the periodic jumps in current due to the tunneling of a single electron. The most likely explanation is that the temperature was not low enough, thus the condition E_C/ggk_BT was not satisfied, and so we were not able to see any discernible features in the data.

Therefore, we then tested our samples in a dilution fridge. The measurements and data of our SETs, taken in a dil fridge at a temperature of 10mK, is presented in the following sections.

5.2 Measurement of Coulomb Blockade in SETs

In order to measure the SETs at temperatures lower than 4K, we perform transport measurements on our sample loaded into a dil fridge. In this section, we present several measurements of Coulomb Oscillations and Coulomb Diamonds with the dil fridge at a base temperature of $\sim$ 10mK. From measurements of the conductance (I/V) and differential conductance (dI/dV)of the SETs, we are able to obtain an estimate for the charging energy and the various capacitances of the SET. Additionally, we also measure the charge sensitivities of these devices.

Coulomb Oscillations: Individual electrons tunneling through the aluminum oxide barrier, hopping onto the island from one lead and off the island to the other lead gives rise to a current flow. This current flow, as described in Chapter 3, is not continuous, but has a peak each time the an additional electron tunnels onto and then off the island. The periodic nature of the current can be seen by fixing the source-

drain voltage and sweeping the gate voltage, which modulates the chemical potential of the island. Fig. 5-1 (a) and (b) present sample data for such Coulomb oscillations in current in one of our SETs. **Coulomb Diamonds:** We can also observe the effect of sweeping both the gate voltage and the bias voltage of the SET. If we plot bias voltage as a function of gate voltage, we see characteristic Coulomb diamonds depicting the coulomb blockade region. In this region no current flows through the SET because the electrons cannot overcome the charging energy of the island. This 2D stability plot is shown in Fig. 5-1 (c) and (d). The DC current measurements measure I vs. V directly, whereas the AC current measurements give a direct measure of dI/dV, which can be seen by taking a Taylor expansion.

Determination of Capacitances from Coulomb Diamonds: From these Coulomb diamonds, we can extrapolate several parameters as described in Chapter 3. We see that the Coulomb diamonds are approximately equally spaced by $\Delta V_g \sim 12mV$, which is the voltage that needs to be applied in order to change the island charge by one electron. The gate capacitance can be obtained from ΔV_g as was calculated in Eq. 3.13. This gives $C_g = e/\Delta V_g \sim 13aF$. The height of the diamond is proportional to the charging energy, giving $E_C = e^2/2C_\Sigma \sim 0.85meV$. A charging energy of $0.85meV$ corresponds to a temperature of $\sim$ 10K. From these two values, assuming that the capacitances of the source and the drain are approximately the same, we get $C_S = C_D \sim 41aF$.

Another way to estimate the source and drain capacitances is using the slopes of the Coulomb Diamond. During our measurement, we ground one of the legs of the SET (the drain) and apply all of our bias voltage to the other leg (the source). The slopes of the Coulomb diamonds are estimated from Fig. 5-1 and using the value for $C_g \sim 13aF$ calculated earlier. The positive slope is estimated to be $V_S/V_g = C_g/(C_g + C_D) \sim 0.85mV/3.7mV \sim 0.2125$ and the negative slope is estimated to be $V_S/V_g = -C_g/C_S \sim -0.85mV/3.2mV \sim -0.2656$. These values of the slopes yield a source capacitance of $C_D = 43aF$ and a drain capacitance of $C_S = 45aF$. Having determined all the capacitances, we can now estimate the charging energy. The total capacitance of the dot is $C_\Sigma = C_1 + C_2 + C_G$. $C = 101aF$ yielding a charging energy

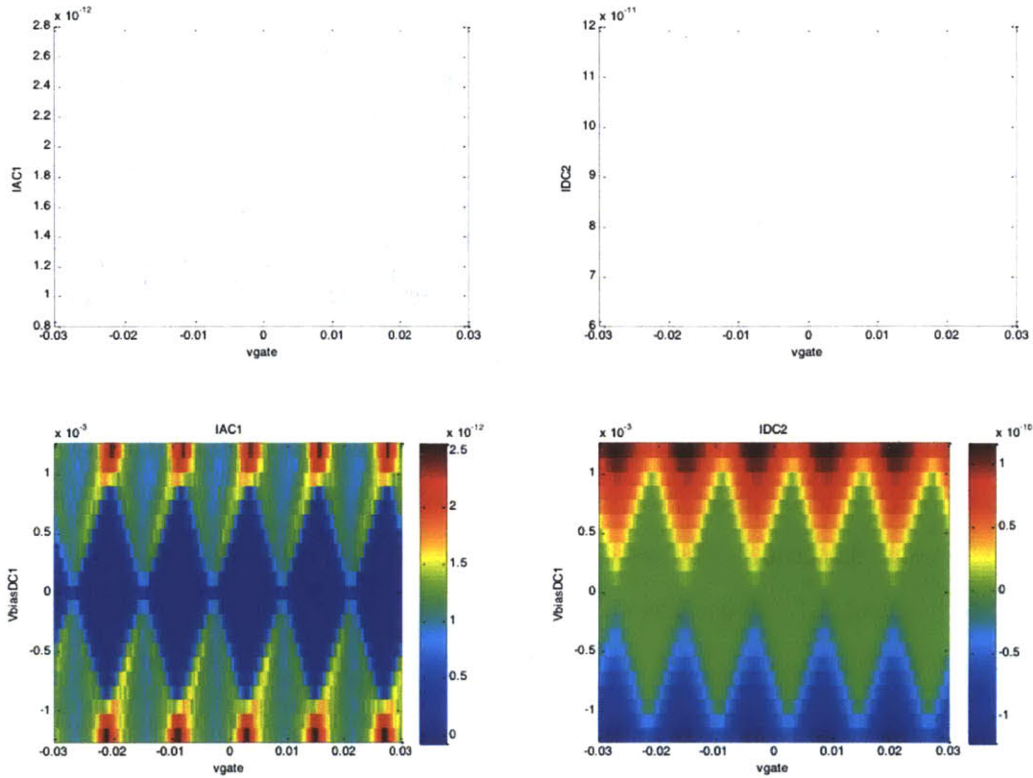

Figure 5-1: (a) is a measure of the AC current (IAC1) for a fixed bias voltage as a function of gate voltage. (b) shows the DC current (IDC1) for the same fixed bias voltage as a function of gate voltage. (c) and (d) are 2D plots showing Coulomb Diamonds. The plots above are line cuts of the Coulomb diamonds for a fixed bias voltage, $V_{SD} = 1.9996 \times 10^{-4}$V. The plots on the left measure the AC current while the plots on the right measure the DC current. The amplitude of the AC bias voltage is $v_{SD} = 9.994 \times 10^{-6}$. (a) and (b) can be thought of as line cuts of the Coulomb diamonds ((c) and (d) respective) for a fixed DC bias voltage.

of $E_C = e^2/2C_\Sigma \sim 0.80meV$. This is approximately the value read off directly from the stability diagram for the diamond height.

5.3 Charge Sensitivity of SETs

Next, I discuss the two different measurements of the charge sensitivity of these SETs.

The typical trace of the dc current as a function of the gate voltage for a fixed bias voltage is shown in Fig. 5-2(b). It shows the Coulomb blockaded regions where the current is zero and the tunneling region where a single electron tunnels across the junction. As the gate voltage is tuned, the current increases from zero, reaches a maximum and decreases again. In order to measure the charge sensitivity, it is necessary to wiggle the system at a given gate voltage by adding a small ac component to the gate voltage. The fluctuations in the voltage generate fluctuations or noise in the current. These current fluctuations are a measure of the susceptibility of the system; the higher the susceptibility the greater the sensitivity of the system.

In the first measurement, the charge sensitivity of the SET is determined by measuring the difference in noise between the current flow and the Coulomb blockade regime. In order to do so, we first fix the bias voltage, V_{SD}. We add a constant AC gate voltage and sweep the DC portion of the gate voltage to measure current through the SET, shown in Fig. 5-2. The plot on the right, (b) shows Coulomb oscillations, i.e. a measure of the DC current through the SET as a function of gate voltage as mentioned above. The plot on the left (a) shows the behavior of the AC current through the SET as a function of gate voltage and is essentially a measure of the noise on the Coulomb oscillations shown in (b). The AC gate voltage induces an electron to tunnel generating the sharp tunneling resonances observed in the AC current. It is interesting to see that the fluctuations are smallest in the blockade region as one might have expected but they are also reduced at the peak of the dc current. The charge fluctuations are maximum on the rise and fall of the dc current which is reasonable because that is when the current is changing the most. The ac signal is therefore sensitive not to the value of the dc current but to the derivative of

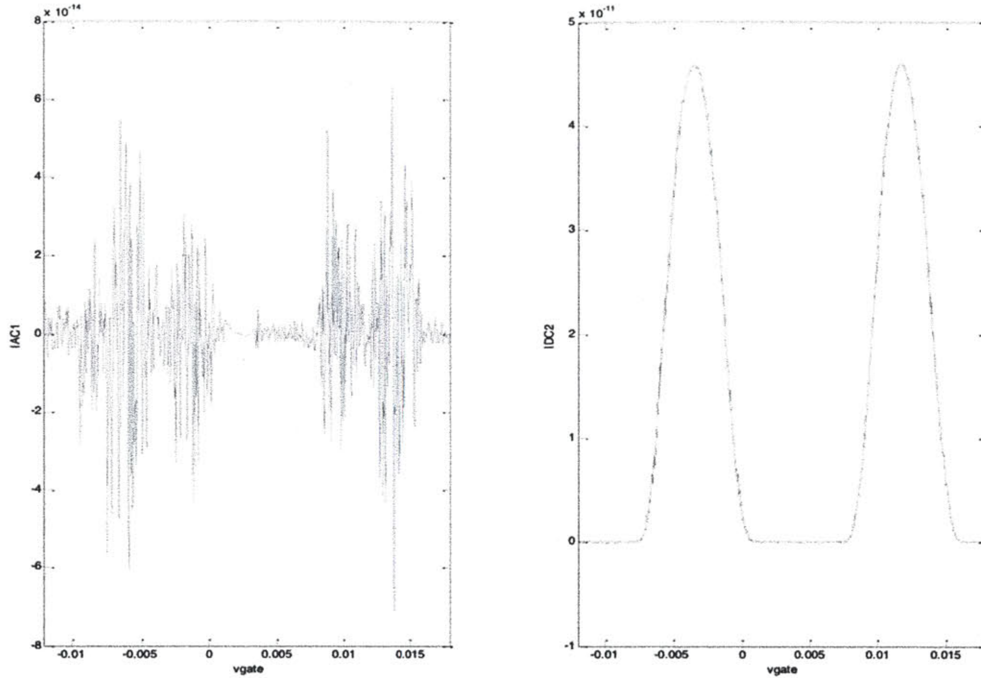

Figure 5-2: (a) Plot of AC current at a frequency of 111HA as a function of gate voltage which illustrates the noise in charge sensitive and charge insensitive regions. (b) Coulomb oscillations of DC current through the SET as a function of gate voltage. This plot is used to determine the range of Vgate in which the SET is sensitive to charge. The DC bias voltage is fixed at $V_{SD} = 0.00039992V$. The gate voltage was modulated with an AC voltage of 9.7968×10^{-7}V.

the dc current.

The noise away from the charge sensitive region is given by the height of the AC current while the gate voltage is such that the SET is in the Coulomb blockade region. This is measured to be apporximately 6 $fA/\sqrt{\text{Hz}}$. The noise in the charge sensitive region is given by the height of the AC current in regions where the gate voltage shows conductance resonances in (b). The noise in this region is seen to be significantly higher, approximately 50 $fA/\sqrt{\text{Hz}}$, and is due to the fact that an electron is tunneling through the tunnel junctions of the SET, enabling current flow. The charge sensitivity is given by converting the noise (units of current per $\sqrt{\text{Hz}}$) into units of charge per $\sqrt{\text{Hz}}$. This is done by first obtaining the slope of the Coulomb oscillation peak, which

gives us current in terms of the gate voltage. Then we use the conversion factor that one charge e corresponds to a change in gate voltage $\Delta V_g = 12mV$ as seen from the Coulomb diamonds. Thus the charge sensitivity is:

$$\frac{noise}{\frac{dI}{dV} * \frac{\Delta V_{gate}}{e}} = \frac{50fA/\sqrt{\text{Hz}}}{1.3 \times 10^{-8}A/V \times 12mV/e} \sim 2.2 \times 10^{-4} \frac{e}{\sqrt{\text{Hz}}}. \tag{5.1}$$

Next we perform a different measurement in order to get another estimate of the noise on the current. In this measurement, the goal is to determine the AC gate voltage at which we will no longer be able to resolve the noise on the DC current through the SET. For this measurement, we fix the bias voltage on the SET and sweep the DC and AC gate voltages while recording the DC and AC current. Fig. 5-3 shows a 2D plot of AC current (left) and DC current(right) as a function of DC gate voltage on the x-axis and AC gate voltage on the y-axis. As we sweep the DC gate voltage, we expect to see a Coulomb oscillation. Fig. 5-3(b) shows this peak in the DC current due to the electron tunneling through the tunnel junctions of the SET. In order to resolve the noise in the current, we modulate the gate voltage (by applying an AC voltage) and look at its effects on the current modulation (by measuring the AC current). When the AC gate voltage is on the order of the noise in the current, we are no longer able to resolve an AC current through the SET. We see from Fig. 5-3 (a) that the AC current signal disappears around 3×10^{-6}V, giving us our noise. We then convert this noise (in units of V) into units of charge, using the conversion factor that one charge e corresponds to a change in gate voltage of $\Delta V_g = 12mV$. Each point is taken for an integration time of 1s. Thus our charge sensitivity is:

$$\frac{noise}{\Delta V_g/e} = \frac{1}{\sqrt{\text{Hz}}} \frac{3 \times 10^{-6}V}{0.012V/e} \sim 2.5 \times 10^{-4} \frac{e}{\sqrt{\text{Hz}}} \tag{5.2}$$

This is a pretty remarkable charge sensitivity, demonstrating why SETs can be used as extremely sensitive charge sensors, as is the case in this experiment.

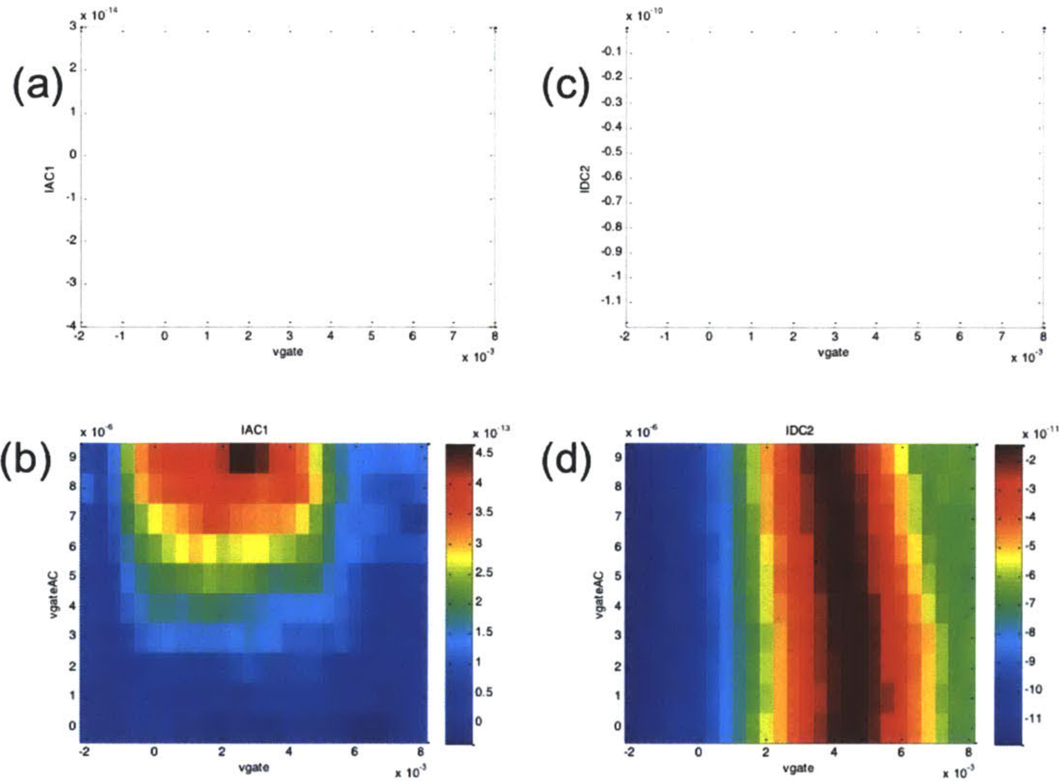

Figure 5-3: Sample measurement used to find noise on current through SET in order to determine charge sensitivity of SET. Bias voltage is fixed at $V_{SD} = -0.001V$. (b) shows a plot of AC current at a frequency of 342Hz as a function of DC gate voltage on the x-axis and AC gate voltage on the y-axis. (d) is a plot of the DC current as a function of DC gate voltage on the x-axis and AC gate voltage on the y-axis. By comparing (b) and (d), we see that below a certain AC gate voltage it is not possible to resolve the AC current.

5.4 Future Testing

The data presented above was taken in a dil fridge at a base temperature of ~10 mK. During the warming up of the dil fridge, we did not have very good control of the temperature, and so were not able to measure these SETs at around 1K or 2K. We ultimately want our SETs to be fully functional at ~2K in a helium cryostat. Once the cryostat arrives at the end of may, we will test these SETs to see if they work at that temperature. But since a charging energy of $0.85meV$ corresponds to a temperature of 10K, we are hopeful that these SETs will show discernible coulomb oscillations with a relatively good charge sensitivity at temperatures of 2K.

Chapter 6

Conclusion

In this thesis, I have described the start of our study of using phosphorus doped silicon as a semiconductor qubit. The ultimate goal of the experiment is to use a novel hybrid technique that combines the advantages of spin selective optical excitations with those of electrical readout measurements to detect the spin state of a single electron. This thesis focuses on the fabrication of SETs which can be used to electrically detect the final charge of the P donor and determine whether the donor remained neutral or was excited and formed a P^+ ion via the Auger process. I have been able to overcome the challenges associated with fabricating SETs that can be operated in the 2K regime. This necessitated minimizing the tunnel junction areas through optimized lithography and evaporation techniques. Through considerable experimentation, I was able to fabricate SETs with very narrow features, the most successful run yielding SETs with 30nm wide legs and a 30nm wide island.

We performed transport measurements in a dil fridge in order to characterize these SET devices. We were able to measure Coulomb oscillations and Coulomb blockade diamonds for these SETs. We find that these SETs have a charging energy of approximately $E_C \sim 0.85$meV which corresponds to a temperature of about 10K. Additionally, we measure the charge sensitivity of the SETs to be $\sim 2 \times 10^{-4} e/\sqrt{\text{Hz}}$. We are pretty confident that these SETs will show discernible Coulomb oscillations with relatively good charge sensitivity at temperatures of 2K. The SETs will be tested in our helium cryostat, in which the experiment will be performed, once it arrives.

SETs are extremely versatile in their applications. They can be used as very sensitive charge detectors as in the larger experiment described in the thesis. They can also be used as very precise temperature sensors as well as magnetometers. Thus the ability to fabricate SETs with higher operating temperatures opens the door to many possible experiments. This could pave the way to further probe fascinating properties of semiconducting systems.

Appendix A

SET Fabrication Recipes

A.1 Photolithography of Optical Gates

Small and Large Gates

- prebake Si wafer 180°C for 3 min
- **Resist LOR 3A**
- Spin 5000 rpm for 40 sec
- Bake 180°C for 5 min
- **Resist S1805**
- Spin 5000 rpm for 40 sec
- Bake 115°C for 5 min
- **Expose** using MA 6 for 4.0 sec
- **Develop** in CD-26 for 60 sec
- Rinse with DI and blow-dry

- **Evaporate**
- 50 Å Ti sticking layer
- 75 Å PdAu
- **Liftoff**
- PG Remover 60°C for 6 hours
- Rinse with DI and blow-dry

Large Gates

- prebake Si wafer 180°C for 3 min
- **Resist LOR 20B**
- Spin 5000 rpm for 40 sec
- Bake 180°C for 5 min
- **Resist S1805**
- Spin 5000 rpm for 40 sec
- Bake 115°C for 5 min
- **Expose** using MA 6 for 4.0 sec
- **Develop** in CD-26 for 60 sec
- Rinse with DI and blow-dry

- **Evaporate**
- 200 Å Ti sticking layer
- 1000 Å Au
- **Liftoff**
- PG Remover 60°C for 6 hours
- Rinse with DI and blow-dry

A.2 Ebeam Lithography

Resist Spinning

- MMA EL3 made by diluting MMA EL6 with Ethyl Lactate in a 1:1 ratio

- **Copolymer MMA EL3**
- Spin 5000rpm 40sec
- Bake 180°C 5 min
- **Resist PMMA A2**
- Spin 5000 rpm 40 sec
- Bake 180°C 5 min
- E-spacer
- Spin 2000 rpm 40 sec
- No bake

Elionix Parameters

- Current = 50pA
- Dose: SET = 0.55, Pads = 0.5, Ucut = 0.2

Development

- Dip in DI H2O for 20sec to remove e-spacer
- Develop in MIBK (sitting on ice for 10 min) for 60sec
- Rinse with IPA and blow-dry

Shadow Evaporation

- Purge O_2 line before beginning evaporation
- Set polar angle to 45°
- Set azimuthal angle parallel to island (evaporation from the right)
- Evaporate 45 Å Al (actually 112 Å due to Xtal monitor conversation)
- Wait 10 min. for metal to cool
- Process gas O_2 at 2.6 mbar, 5.5 min
- Set azimuthal angle parallel to legs (evaporation from the top)
- Evaporate 65 Å Al (actually 162 Å due to xtal monitor conversion)
- Wait 10 min for metal to cool

- Liftoff in boiling acetone

Bibliography

[1] N.W. Ashcroft and N.D. Mermin. *Solid State Physics.* Saunders College Publishing, Fort Worth, 1976.

[2] M. H. Devoret and R. J. Schoelkopf. Amplifying quantum signals with the single electron transistor. *Nature*, 406:1039–1046, 2000.

[3] G. J. Dolan. Offset masks for lift-off photoprocessing. *Applied Physics Letters*, 31:5, 1977.

[4] A. Yang et. al. Optical detection and ionization of donors in specific electronic and nuclear spin states. *Phys. Rev. Lett*, 97:227401, 2006.

[5] B. E. Kane et. al. Single spin measurement using single-electron transistors to probe two-electron systems. *Phys. Rev. B.*, 61:2961, 2000.

[6] L. Kouwenhoven et. al. Single electron charging effects in semiconductor quantum dots. *Z. Phys. B - Condensed Matter*, 85:367–373, 1991.

[7] T. A. Fulton and G. J. Dolan. Observation of single-electron charging effects in small tunnel junctions. *Phys. Rev. Lett*, 59:109, 1987.

[8] G. Grosso and G.P. Parravicini. *Solid State Physics.* Elsevier Academic Press, Amsterdam, 2000.

[9] S. Hickman. Liftoff photoresist processing. `cns.fas.harvard.edu/facilities/docs/SOP112_r1_1_\%20LOR.pdf`.

[10] T. Ihn. *Semiconductor Nanostructures - Quantum States and Electronic Transport.* Oxford University Press, New York, 2010.

[11] B. E. Kane. A silicon-based nuclear spin quantum computer. *Nature*, 393:133, 1998.

[12] M. A. Kastner. Artificial atoms. *Physics Today*, 46:24, 1993.

[13] M. A. Kastner. The single electron transistor and artificial atoms. *Annalen der Physik*, 9:885–894, 2000.

[14] C. Kittel. *Introduction to Solid State Physics.* John Wiley and Sons, Amsterdam, 8th edition, 2005.

[15] L. Kouwenhoven and C. Marcus. Quantum dots. *Physics World*, 1998.

[16] Y. Nakamura, C. Chen, and J. Tsai. 100-k operation of al-based single electron transistors. *Japan Appl. Phys.*, 35:1465–1467, 1996.

[17] Y. A. Pashkin, Y. Nakamura, and J. S. Tsai. Room-temperature al single-electron transistor made by electron-beam lithography. *Applied Physics Letters*, 76:16, 2000.

[18] M. Y. Simmons. Probing dopants at the atomic level. *Nature Physics*, 4:165, 2008.

[19] D. Sleiter, N. Y. Kim, K. Nozawa, T.D. Ladd, M. L. W. Thewalt, and Y. Yamamoto. Quantum hall charge sensor for single-donor nuclear spin selection in silicon. *New Journal of Physics*, 12, 2010.

[20] L. Sohn, L. Kouwenhoven, and G. Schon, editors. *Mesoscopic Electron Transport.* Kluwer Academic Publishers, Dordrecht, 1997.

[21] Silicon Crystal Structure. `http://hyperphysics.phy-astr.gsu.edu/hbase/solids/sili2.html`.

[22] A. M. Tyryshkin, S. A. Lyon, A. V. Astashkin, and A. M. Raitsimring. Electron spin relaxation times of phosphorus donors in silicon. *Phys. Rev. B*, 68:193207, 2003.